2022

Reporter Chondrocyte Optimization of Bioinks for Zonal 3D Bioprinting of Cartilage

Kari Martyniak
University of Central Florida

REPORTER CHONDROCYTE OPTIMIZATION OF BIOINKS FOR ZONAL 3D BIOPRINTING OF CARTILAGE

by

KARI MARTYNIAK
M.S. University of Central Florida, 2016
B.A. The College of Wooster, 2013

A dissertation submitted in partial fulfillment of the requirements
for the degree of Doctor of Philosophy
in the Department of Biomedical Sciences
in the College of Medicine
at the University of Central Florida
Orlando, Florida

Fall Term
2022

Major Professor: Thomas J. Kean

ABSTRACT

Osteoarthritis (OA) is the most common form of arthritis, often thought of as a disease of the elderly, but post traumatic OA predominantly impacts younger individuals. Articular cartilage is the tissue that coats the end of your bones in synovial joints. Since cartilage has limited healing capacity, defects, or injuries to it progressively erodes down to the subchondral bone. Unfortunately, current treatment options all have limitations, particularly for younger patients. Cartilage has a specific zonal architecture that is distinguished by the different cell morphologies and arrangements, biochemical composition, and mechanical properties. 3D bioprinting is a tissue engineering technique that involves the simultaneous extrusion of biomaterials and cells to fabricate constructs. The layer-by-layer nature of 3D bioprinting and the frequent use of hydrogels as biomaterials make it a promising technique to engineer zonal articular cartilage. The goal of this dissertation was to develop and use novel human reporter chondrocytes to determine optimal combinations of biomaterials to 3D bioprint both the middle-deep and surface zones of articular cartilage. Human articular chondrocytes were transduced with either a type II collagen promoter- or lubricin promoter-driven *Gaussia* luciferase. Upon promoter stimulation, luciferase is secreted by the cells enabling a high-throughput, temporal, assessment of either type II collagen or lubricin. The human chondrocyte reporter system was combined with a Design of Experiment approach which streamlined the process of biomaterial optimization. To 3D bioprint the deep zone, an optimal combination of gelatin methacrylate (GelMA) and hyaluronic acid methacrylate (HAMA) was determined based on type II collagen promoter-driven luminescence, chondrocyte mobility and biomaterial stiffness. While an optimal combination of GelMA and oxidized methacrylated alginate (OMA) was determined for the surface zone based on lubricin

promoter-driven luminescence, lubricin secretion, and construct shape fidelity. Together these results highlight the effectiveness of human reporter chondrocyte optimization for 3D bioprinting zonal cartilage.

Dedicated to my mom and brother.

ACKNOWLEDGMENTS

First and foremost, I'd like to express my gratitude to Dr. Kean, for his belief in me, support, and guidance. I'd also like to thank my committee members: Drs. Masternak, Willenberg and Perotti, for their support and expertise.

I'd like to acknowledge the members of the Kean lab both past and present. Specifically, Alesia Lokshina, Sean Kennedy, Makan Karimzadeh and Rachel Kemp for their contributions to this dissertation. Also, Dr. Maria Cruz, who was always willing to help me plan experiments, double check calculations, change nitrogen tanks, and share funny dog videos or Modern Family quotes.

I'd also like to give a big thank you, full of appreciation to all my friends who've supported and encouraged me throughout this process. You all are the absolute best, and I couldn't have done this without you.

Finally, I like to thank my mom and brother for their love, encouragement, and signature brand of humor.

TABLE OF CONTENTS

LIST OF FIGURES

LIST OF TABLES

LIST OF ACRONYMS (or) ABBREVIATIONS

BSA	Bovine Serum Albumin
COL2A1	Type II collagen alpha 1 chain
DMA	Dynamic mechanical analysis
DMEM-LG	Dulbecco's Modified Eagle Medium – Low Glucose
DMEM-HG	Dulbecco's Modified Eagle Medium – High Glucose
DMMB	Dimethylmethylene blue
DMSO	Dimethyl sulfoxide
DoE	Design of experiment
ECM	Extracellular matrix
EDTA	Ethylenediaminetetraacetic acid
ELISA	Enzyme-linked immunosorbent assay
F12	Ham's F12 Media
FBS	Fetal Bovine Serum
basic FGF	Basic Fibroblast Growth Factor, Fibroblast Growth Factor 2
GAG	Glycosaminoglycan
GelMA	Gelatin methacrylate
GFP	Green Fluorescent Protein
HAMA	Hyaluronic acid methacrylate
HDP	Hydroxyproline
HuChon-GFP	Green fluorescent transduced human articular chondrocytes
HuCOL2gLuc	Type II collagen promoter-driven *Gaussia* luciferase human articular chondrocytes

HuPRG4gLuc	PRG4 promoter-driven *Gaussia* luciferase human articular chondrocytes
ITS	Insulin, Selenium, Transferrin
LAP	Lithium phenyl-2,4,6-trimethylbenzoylphosphinate
MA	Methacrylic Anhydride
MEM	Minimal Essential Media
MMP	Matrix metalloproteinases
OA	Osteoarthritis
OMA	Oxidized methacrylate alginate
PBS	Phosphate buffered saline
PRG4	Proteoglycan 4; Articular Superficial Zone Protein; Lubricin
PTOA	Post traumatic osteoarthritis
qPCR	Quantitative Reverse Transcriptase Polymerase Chain Reaction
RCF	Relative Centrifugal Force; G - gravity
RGD	Arginine-Glycine-Aspartic acid
RLU	Relative Light Units
RT	Room Temperature
TGFβ1	Transforming Growth Factor Beta 1

CHAPTER 1: INTRODUCTION

Osteoarthritis

Osteoarthritis (OA) is the most common form of arthritis, negatively impacting millions of individuals each year [1–3]. Articular cartilage has limited healing capabilities, therefore defects to this tissue continue to degenerate over time. Several potential factors have been implicated as causes of this degenerative joint disease including age, gender, family history of OA, systemic inflammatory diseases or trauma [4]. Early diagnosis of OA poses a challenge however, as changes to the cartilage at this point do not cause pain, due to the aneural nature of the tissue [5]. Thus, this disease is often not caught until the advanced stages. While OA has traditionally been thought of as a disease of the elderly, ~12% of all OA cases are post traumatic osteoarthritis (PTOA), which mainly affects younger individuals [6]. PTOA is one instance where early intervention is possible [7].

Unfortunately, there are limited treatment options for younger individuals. Palliative care is the first step, aimed at managing the pain and inflammation, however, surgical intervention is often necessary. Surgical strategies include abrasion chondroplasty and microdrilling that are aimed at stimulating spontaneous repair from the subchondral bone, but results are often fibrous cartilage and highly variable [1]. Allografting has the limitation of available tissue and the risk of an immune response [1]. Autografting involves taking healthy tissue from a secondary site, creating lesions at the harvest sites [1]. Autologous-chondrocyte implantation utilizes healthy chondrocytes isolated from the patient, which are then expanded *in vitro* and are then introduced to the defect site under a periosteal flap either alone or embedded in a matrix (matrix induced

autologous-chondrocyte implantation) [1]. The drawbacks to these procedures are they involve two separate surgeries, and still create a secondary surgical site where the healthy chondrocytes are harvested [1]. Current treatments improve short term outcomes, but fully functional restoration of articular cartilage is hard to achieve.

Articular Cartilage

Articular cartilage is a highly specialized connective tissue that coats the ends of the bones in synovial joints. It functions as a frictionless surface for movement and assists in the distribution of loads [8]. Cartilage is composed of only chondrocytes and extracellular matrix (ECM) making it aneural, avascular and devoid of lymphatics [8]. Chondrocytes develop, maintain and repair the ECM which is composed mainly of collagen and proteoglycans, saturated with water [8]. This microenvironment means chondrocytes rarely form cell-to-cell contacts for signaling, but they do respond to stimuli including growth factors and mechanical [8]. Adult chondrocytes have a limited ability to replicate, a significant factor contributing to articular cartilages' limited healing capacity.

Chondrocyte Mobility

Articular chondrocytes are typically considered to be immobile due to the dense ECM [9]. Previous studies have demonstrated that articular chondrocytes will migrate in response to various stimuli *in vitro* [10–12]. These studies have mostly relied on 2D culture and only a few have shown chondrocyte mobility in 3D culture [13–15]. Chondrocyte mobility has been observed in a 3D "dot" of 4% type I collagen in response to nitric oxide [13], and in a mixture of

type I collagen and hyaluronic acid [14]. A cartilage defect wound healing model using a disc of collagen type I and II containing chondrocytes with a 5mm defect, showed migration into the defect area over 4-weeks [15]. These studies indicate chondrocytes do have the capacity to move, and this ability may be essential for defect wound healing, or integration of 3D bioprinted implants.

Zonal Articular Cartilage Organization

Native articular cartilage has a very specific zonal organization that is important for physiological function (Fig. 1) [16]. The zones can be distinguished by the different cell morphologies and arrangements, biochemical composition and mechanical properties (Fig. 1) [16]. Articular cartilage can be divided into four separate zones: surface, middle, deep and calcified [8,17].

The surface or superficial zone constitutes about 10-20% of articular cartilage thickness and functions to protect the deeper layers from shear stress [8,17]. In this layer both the collagen fibers (type II and IX) and chondrocytes are oriented parallel to the articulating surface [8,17,18]. There are a higher number of chondrocytes in this zone with a flat morphology [8,17].

The middle zone is the transition zone between the surface and deep zone [8]. The collagen fibers have a more random orientation but are also thicker than in the surface zone [17]. It constitutes 40-60% of articular cartilage thickness and functions as the first layer of resistances to compressive forces [8,17]. However, most of the compression resistance comes from the deep

zone. This zone has the highest proteoglycan content, lowest water concentration, and the chondrocytes have a rounded morphology arranged in columns perpendicular to the articulating surface [8,17]. The largest diameter collagen fibers are found in this deep zone and are also oriented perpendicular to the articulating surface [8,17].

The calcified zone is where the cartilage is secured to the subchondral bone [8]. It is separated from the deep zone by a tide mark, but the thick collagen fibers of the deep zone are anchored down into the bone [8,17]. The gradual change in matrix/tissue properties confer the ability to cushion the joints and distribute load across the bone.

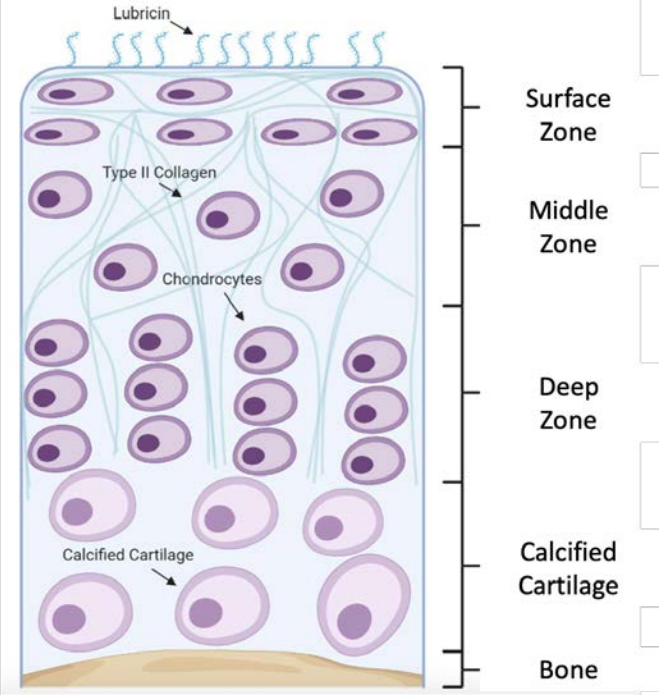

Figure 1: Zonal architecture of articular cartilage (Adapted from [19])

Extracellular Matrix (ECM)

Type II Collagen

Articular cartilage structure and strength depends on the crosslinking of different collagens and changes to their size and orientation depending on the zone they reside in [20]. Several types of collagen are present throughout articular cartilage but, type II collagen is the most abundant, comprising 90-95% of the total collagen [8,17,20]. Type II collagen forms the core fiber network by crosslinking with collagens IX and XI [20]. This complex contributes to articular cartilage resistance to compression and tensile properties [8]. Unfortunately, it is difficult to achieve native levels of expression of type II collagen *in vitro* [21,22]. Tissue engineered cartilage has been documented to have type II collagen content only 25% [23], 20% [21,24], or even 10% [25,26] that of native tissue. This results in diminished biomechanical properties as compared to native tissue, a problem that has yet to be resolved.

Aggrecan

Proteoglycans are the heavily glycosylated monomers that are the most abundant protein after collagens [8]. Structurally these molecules have a central core protein which then has linear glycosaminoglycan (GAG) chains attached [8,27]. Aggrecan is the most abundant proteoglycan found in articular cartilage, and nearly 90% of its mass is comprised of chondroitin sulfated GAG chains [27]. Aggrecan is found in between the collagen fiber complexes of the ECM and its key role is creating osmotic swelling pressure by drawing water into the tissue [8,27]. The GAG side chains have negatively charged anionic groups, which sodium ions attach to [27]. This creates an ion concentration gradient, and an imbalance between cartilage and the surrounding

tissues, resulting in water being drawn into the cartilage tissue [8,27]. Aggrecan also creates a stiff network with the collagen fibers, adding to the strength of the tissue [27]. The water swollen matrix, along with additional structural support give articular cartilage its viscoelastic mechanical property [27]. This means cartilage has structural resistance upon sudden impact, but also retains its elastic behavior under sustained loads [27].

Lubricin

Chondrocytes in the surface zone of articular cartilage synthesize and secrete lubricin [8,17,18]. Lubricin is a proteoglycan, derived from the proteoglycan 4 (*PRG4*) gene, which functions as a boundary lubricant and anti-inflammatory agent [28,29]. It has been shown to decrease the coefficient of friction [30] and prevent synovial cell and protein adhesion to the cartilage surface [31]. It is essential for fully functional articular cartilage, and mutations to the *PRG4* gene result in camptodactyly-arthropathy-coxa vara-pericarditis syndrome, a disease resulting in alteration of the articular surface and cartilage degeneration [29,32]. Treatment with recombinant lubricin, or lubricin mimetics have been shown to reduce the damaging effects of surgically induced OA in rats [33,34] and OA in ovariectomized rats [35]. Increasing lubricin expression is a promising method for treating OA. Especially because the surface zone of articular cartilage is the first area impacted by cartilage defects [28,36,37]. Defects occur in the superficial layer, and continue to erode down through each layer to the sub-chondral bone [17].

3D Bioprinting

Tissue engineering is an interdisciplinary field that aims to develop structural and functional alternatives for native tissue [38,39]. The ideal tissue engineered cartilage construct will mimic native ECM, encapsulate cells, and not only fill and maintain the defect space while the new tissue grows, but also enable integration with the surrounding native tissue [40]. 3D bioprinting has the potential to achieve an ideal tissue engineered construct through the simultaneous extrusion of both living cells and biomaterials [41,42]. Extrusion based 3D bioprinting is the most widely used type of 3D bioprinting for cartilage constructs [43]. Advantages of this method include the ability to print patient specific bioactive scaffolds and recapitulation of native tissue zonal architecture, because of the layer-by-layer printing process [41,44]. Post-fabrication cell-seeding is not required, and tissue is therefore not hindered by limited cell penetration [45]. Since the cells are encapsulated within the biomaterial, material selection is an imperative first step for 3D bioprinting.

Biomaterials

Properties of biomaterials used for 3D bioprinting directly impact cell viability, gene expression and construct mechanical properties. Biomaterial printing requirements like temperature, time, oxygen and nutrient availability need to be considered when choosing which materials to work with [42,46]. Gelation or crosslinking methods also need to fulfill the basic requirement of biocompatibility while still enhancing the mechanical properties and stability of the biomaterials [46]. Hydrogels are the most common biomaterials used for 3D bioprinting cartilage [43]. Hydrogels are biocompatible and can be used to mimic cartilage ECM because of their water

binding [47]. Their biological properties can aid in cell adhesion, proliferation, migration and differentiation, and their mechanical properties make them highly printable [17,48,49].

Gelatin Methacrylate (GelMA)

Gelatin is a hydrolysis product of collagen which contains cell adhesion arginine-glycine-aspartic acid (RGD) sites, and target degradation sequences for matrix metalloproteinases (MMP) that enable remodeling [50,51]. It is a natural polymer with low antigenicity and has been shown to be resorbable *in vivo* [52]. The drawback of gelatin is that it melts at physiological temperatures, however, methacrylation enables photocrosslinking and increases its stability and mechanical properties. Gelatin methacrylate (GelMA) is synthesized through the reaction of gelatin with methacrylic anhydride (MA) (Fig. 2) [50]. The reaction results in a methacryloyl group substitution on the amine and hydroxyl groups of amino acid residues (Fig. 2) [50]. Differing degrees of substitution can be achieved through varying the amount of MA in the reaction and adjusting the pH of the reaction [50]. Gelatin methacrylate (GelMA) is one of the most frequently used biomaterials for 3D bioprinting cartilage because of its advantageous biological properties and tunable mechanical properties [43].

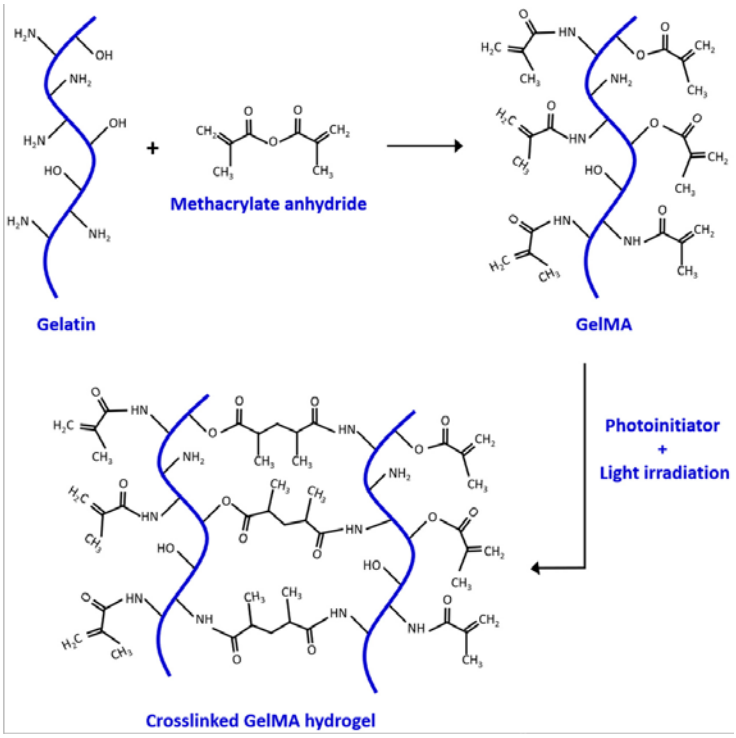

Figure 2: Synthesis of gelatin methacrylate and subsequent photocrosslinking (Adapted from [53])

Hyaluronic Acid Methacrylate (HAMA)

Hyaluronic acid is an integral GAG of cartilage ECM, and is found abundantly in synovial fluid [54]. It has been shown to provide cells with biochemical cues mediated by receptors CD44 and RHAMM, and to regulate cell morphology, proliferation and migration [54]. It has also been shown to promote stem cell differentiation towards the chondrogenic lineage [54]. Hyaluronic acid can be easily modified to add methacrylate groups through a reaction with methacrylic anhydride resulting in methacryloyl group substitution on the hydroxyl groups (Fig. 3) [55]. A drawback to using HAMA alone is that it had no natural cell binding motifs, and limited cell spreading has been observed [56,57]. In this dissertation, this was overcome by mixing GelMA and HAMA together.

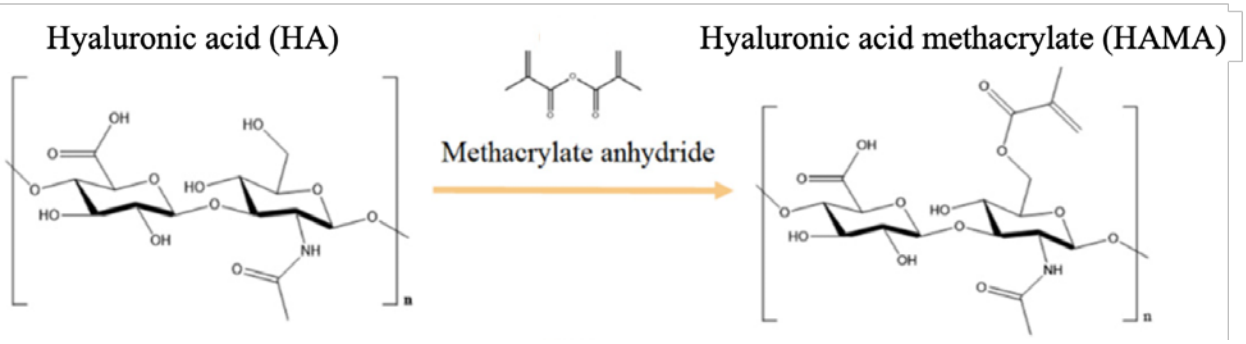

Figure 3: Synthesis of hyaluronic acid methacrylate (Adapted from [58])

Oxidized Methacryalted Alginate (OMA)

OMA is chemically modified alginate developed for its controllable mechanical properties [59,60]. Alginate alone is not naturally degradable but the oxidation of alginate by sodium periodate, prior to methacrylation alters the uronate residue conformations, making it more vulnerable to hydrolysis and creating tunable degradation rates (Fig. 4) [60]. It has been shown to be ideal for 3D bioprinting due to its shear-thinning and self-healing ability after calcium crosslinking [61]. Secondary crosslinking through photocrosslinking of the methacrylate groups, further increases the biomaterials' stability after printing [61]. OMA has been shown to be biocompatible and able to be printed with high fidelity [60–62].

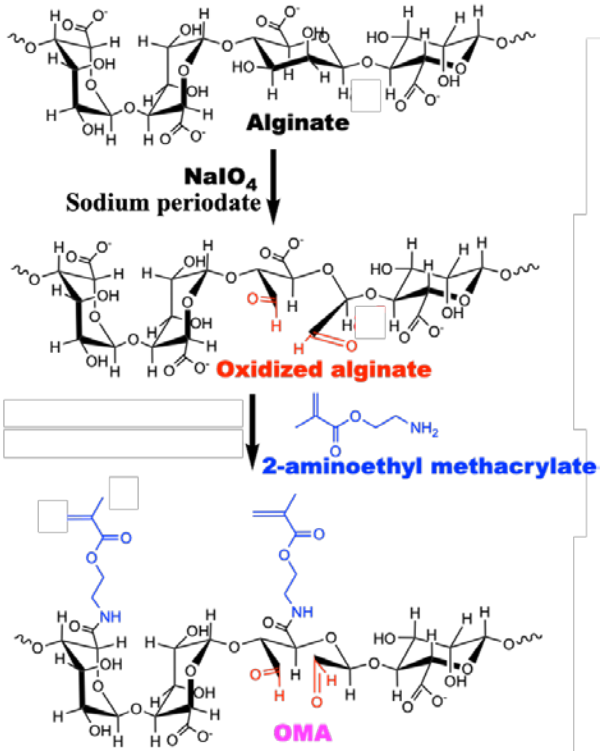

Figure 4: Synthesis of oxidized methacrylated alginate (OMA)

Lithium phenyl-2,4,6-trimethylbenzoylphosphinate (LAP) Photocrosslinker

Methacrylation of the previously described materials enables photocrosslinking to increase stability and stiffness. Lithium phenyl-2,4,6-trimethylbenzoylphosphinate (LAP) is a commonly used photoinitator. The reaction occurs when the photoinitiator LAP absorbs light which stimulates its decomposition and release of free radicals that then facilitate the crosslinking of the methacrylate groups, by reacting with the carbon-carbon double bonds present on the methacryloyl modification on the biomaterials (Fig. 2) [63]. An advantage of LAP is that it can crosslink at 405nm (visible light), thereby reducing DNA damage by UV light [64]. Cells have been shown to have high viability (~79%) in a 10% GelMA solution with 0.5% LAP [64,65].

Engineered Human Articular Chondrocyte Reporter Cells

An essential aspect of chondrocyte culture is characterizing and quantifying chondrogenesis. Unfortunately, end-point assays are typically performed to assess this. Relying on qPCR, biochemical assays or histology are all beneficial but destroy the construct or cells in the process. To allow for temporal assessment, ATDC5s were engineered through lentiviral transduction of *Gaussia* luciferase under control of the *COL2A1* promoter [22]. *Gaussia* luciferase is secreted from the cells upon promoter stimulation making this a non-destructive, high-throughput, and easy to use assay. The type II collagen reporter system has been used and characterized in ATDC5 cells for micronutrient optimization of chondrogenic media [22]. This data when combined with traditional end-point assays establishes a more in-depth characterization of the chondrogenic response. Human articular chondrocytes were engineered to assess type II collagen [22,66] or lubricin [19] expression and this dissertation characterizes those matrix driven reporter cells and demonstrates their use in biomaterial optimization.

Design of Experiment (DoE)

Design of Experiment (DoE) software (Design-Expert, Stat-Ease) was used in this study to aid in streamlining the process of biomaterial selection for 3D bioprinting cartilage. The DoE is a well-established technique for planning experiments using the minimum number of test groups to generate the maximum amount of information [67,68]. Test groups are generated using statistical modeling based on input parameters and the desired outputs. A mixture design approach is an established [67–69] and efficient method to investigate optimal biomaterials. The key feature of

a mixture design is that the sum of all components adds up to 100% [68]. Therefore, the factors within the mixture cannot be changed completely independent of each other, the proportions to one another will be between 0 and 1 [68]. A screening is used to investigate a large number of mixtures, aiming to reveal which factors are the most important [68]. This method is advantageous when optimizing biomaterial selection as it can reduce the amount of materials used and the time it traditionally takes for optimization.

Dissertation Overview

Our overall hypothesis is that zonal articular cartilage specific ECM gene expression can be stimulated by biomaterials, which can be studied and optimized using primary human chondrocyte reporters. A challenge in 3D bioprinting is identifying and optimizing biomaterials for desired gene expression. Traditional methods used to determine biomaterial impact on ECM gene expression rely on end point assays. To test our hypothesis, primary human chondrocytes were transduced with either type II collagen promoter- or lubricin promoter-driven *Gaussia* luciferase. In Chapter 3, an optimal ratio of GelMA and HAMA for the middle-deep zone of articular cartilage was determined based on type II collagen promoter-driven luminescence, chondrocyte mobility and biomaterial storage modulus. In Chapter 4, an optimal combination of GelMA and OMA for the surface zone of articular cartilage was determined based on lubricin promoter-driven luminescence, biochemical and mechanical data. Together these results are the building blocks for recreating the zonal architecture of native articular cartilage through 3D bioprinting, while also demonstrating the advantages of using a DoE approach and the human chondrogenic ECM reporter system.

CHAPTER 2: MATERIALS AND METHODS

Human Chondrocyte Isolation

Human articular chondrocytes were isolated from discarded surgical tissue collected from two patients during total joint replacement surgery with informed consent under IRB approved protocols (Baylor College of Medicine, H-36683, H-36374). Discarded tissue < 3h post-operation on ice in saline) was briefly stored in defined chondrogenic media (DMEM-HG 93.24% (Lonza), 1% 10^{-5}M dexamethasone (Sigma), 1% ITS+premix (Becton-Dickinson), 1% Glutamax (Hyclone), 1% 100 mM Sodium Pyruvate (Hyclone), 1% MEM Non-Essential Amino Acids (Hyclone), 0.26% 50mM L-Ascorbic Acid Phosphate (Wako), 0.5% Fungizone (Life Technologies)). Cells were plated in non-adherent 96-well sterile plates (Greiner Bio), ~4h, room temperature [RT]) [70]. Visually intact cartilage tissue was dissected from the femoral condyle using sterile technique (~3cm x 1cm) and diced into pieces <1mm^3 in DMEM-LG (Hyclone). Diced tissue was centrifuged (1 min, 100 RCF, RT), supernatant removed, and digested in hyaluronidase enzyme solution (40 mL, 660 Units/mL in DMEM-LG/F12, Sigma,) for 30 minutes (37°C) on a nutating rocker and then centrifuged again. After the supernatant was removed, collagenase type II was added (40 mL, 583 Units/mL in DMEM/F12 with 10% FBS, Worthington Biochemical Corp CLS2) for overnight digestion (15h). Remaining fragments were removed (70 µm Nitex filter) and the cell suspension diluted 1:1 with DMEM/F12 before centrifugation (10 min, 700 RCF, RT). Cells were resuspended in growth media (DMEM/F12 supplemented with 10% FBS (mesenchymal stromal cell selected [71] and 1% penicillin-streptomycin). Live cells were cryopreserved or transduced as described below.

Engineering of Type II Collagen Promoter-Driven Reporter Human Chondrocytes (HuCOL2gLuc), PRG4 Promoter-Driven Human Chondrocytes (HuPRG4gLuc) and GFP Chondrocytes (HuChon-GFP)

Lentiviral plasmids (type II collagen - HPRM22364-LvPG02, lubricin - HPRM34762-LvPG02, EX-EGFP-Lv105, psPAX2 and pMD2.G) were grown in E-Coli (GCI-L3, GeneCopoeia, Inc.) and column purified (Qiagen Maxiprep) before co-transfection into HEK-293Ta cells (GeneCopoeia, Inc.) [22]. Col2gLuc, PRG4gLuc or GFP pseudolentiviral particles were collected from supernatant and concentrated by centrifugation (10,000 RCF, 4°C, overnight [22]). Freshly isolated human chondrocytes were seeded (6,100 cells/cm^2) in growth media and allowed to adhere overnight to a 10cm cell culture dish. Chondrocytes were then incubated with Col2gLuc, PRG4gLuc or GFP pseudolentiviral particles (multiplicity of infection (MOI) ~25) in Opti-MEM (Gibco) containing polybrene (4 µg/mL) at 4°C for 15 min before placing at 37°C overnight (5% CO_2, 5% O_2, 17h). Following overnight incubation, pseudolentiviral particle containing media was removed and replaced with growth media. Chondrocytes were grown to 70-90% confluence before trypsinization and seeding onto synoviocyte matrix coated flasks [72,73]. Synoviocyte matrix coated flasks were used due to their ability to dramatically increase cell yield while retaining chondrogenesis. HuCOL2gLuc cells were grown until at ~90% confluence, cells were trypsinized, neutralized and cryopreserved in FBS (95%) with DMSO (5%). HuPRG4gLuc cells were grown to ~90% confluence and then passaged onto synoviocyte matrix coated flasks and isolated with puromycin (2 ug/mL) for 7 days. The remaining cells were grown to ~90% confluence prior to being trypsinized, neutralized, and cryopreserved with FBS (95%) and DMSO (5%). HuChon-GFP infected chondrocytes were assessed by microscopy (Zoe™ imager, Bio-Rad) as shown in the results (Fig. 12E).

Reporter Cell Aggregate TGFβ1 Dose Response

HuCOL2gLuc or HuPRG4gLuc infected chondrocytes were assessed through dose response to TGFβ1 to establish the cells as chondrogenic reporters. Reporter chondrocytes were thawed from frozen stocks, seeded onto synoviocyte derived matrix coated flasks and expanded to confluence. At confluence, cells were trypsinized (0.25% Trypsin/EDTA, 5 min, 37°C), neutralized with growth media, then centrifuged (5 min, 500 RCF, RT). Supernatant was removed and cells resuspended in defined chondrogenic media (DMEM-HG 93.24% (Lonza), 1% 10^{-5}M dexamethasone (Sigma), 1% ITS+premix (Becton-Dickinson), 1% Glutamax (Hyclone), 1% 100 mM Sodium Pyruvate (Hyclone), 1% MEM Non-Essential Amino Acids (Hyclone), 0.26% 50mM L-Ascorbic Acid Phosphate (Wako), 0.5% Fungizone (Life Technologies)). Cells were plated in non-adherent 96-well sterile plates (Greiner Bio), TGFβ1 added (0-100 ng/mL for HuCOL2gLuc and 0-40 ng/mL for HuPRG4gLuc, Peprotech) and centrifuged into aggregates (5 min, 500 RCF, RT). Cell aggregates were incubated for 3 weeks with media exchange every 2-3 days (37°C, 5% CO_2 and 5% O_2). Conditioned media, containing the secreted *Gaussia* luciferase, was assessed for luminescence every 2 days. On day 22, cell aggregates were divided between histological, biochemical assessment or qPCR (HuPRG4gLuc aggregates only). Culture media was saved and frozen (-20°C) on days 1, 10 and 22 from the HuPRG4gLuc cells for lubricin ELISA.

Reporter Cell qPCR Assessment

HuCOL2gLuc infected chondrocytes were cultured in a monolayer on 12-well cell culture plate (Corning) for qPCR gene assessment. Cells were seeded (6,100 cells/cm^2) in growth media and allowed to adhere overnight. Then growth media was replaced with chondrogenic media supplemented with 0-10ng/mL TGFβ1. By day 5, luciferase assessment of culture media showed a dose response in luminescence values. Cells were extracted for RNA analysis with lysis buffer (Ambion PureLink RNA Mini kit) and the lysate frozen on dry ice and stored (-80°C, 1 week). Cell aggregates (n = 5) from HuPRG4gLuc TGFβ1 dose response were frozen in RNA lysis buffer on day 22. Total RNA was isolated from lysates using column purification with on-column DNA digest. RNA purity and integrity was assessed by RNA ScreenTape (Agilent Technologies). cDNA was synthesized from RNA using a cDNA synthesis master mix (Maxima H Minus, Thermo Scientific). qPCR was performed (QuantStudio 7 flex, Applied Biosystems) for gene expression of Hypoxanthine Phosphoribosyltransferase 1 (*HRPT*, reference gene, forward primer: 5' ATTGACACTGGCAAAACAATGC 3', reverse primer: 5' TCCAACACTTCGTGGGGTCC 3', [72]), Gaussia luciferase (gLuc, 5' ACGCTGCCACACCTACGA 3', reverse primer: 5' CCTTGAACCCAGGAATCTCAG 3' [22]) and type II collagen (*COL2A1*, 5' TGGAGACTACTGGATTGACCCCAACCAA 3', reverse primer: 5' TCTCGCCAGTCTCCATGTTGCAGA 3' [72]) or lubricin (*PRG4*, forward primer: 5' TTGCTCCTCTCTGTTTTCGT 3', reverse primer: 5' ATACCCTTCCCCACATCTCCC 3'). Primers, SYBR green (Applied Biosystems, Thermofisher Scientific) and cDNA were mixed and run using cycling parameters: 95°C for 20s then 45 cycles of 95°C 10s, 60°C 20s, 72°C 19s, followed by melt curve analysis. CT values were normalized to *HRPT* expression and then gLuc

vs. *COL2A1* and gLuc vs. *PRG4* relative gene expression was plotted with 95% confidence bands (GraphPad Prism).

Preparation of Biomaterial Combinations

Biomaterials for Middle-Deep Zone

GelMA (45-55% methacrylated, Cellink) and HAMA (30% methacrylated, molecular weight of 63 kDa via multi-angle laser light scattering, Sigma) stocks were made in Tyrode's (Sigma) containing 0.05% lithium phenyl-2,4,6-trimethylbenzoylphosphinate (LAP, Cellink). GelMA stock (15% w/v) was prepared with prewarmed Tyrode's (~40°C) on a hotplate stirrer. HAMA stock (2% w/v) was prepared in Tyrode's at room temperature. All stocks were stored in the dark at 4°C until use. To prepare biomaterial combinations, hydrogel components were mixed at 40°C using volume ratios (Table 1). Biomaterials were then cooled to ~37°C, the cell suspension added and mixed by vortexing. The final cell concentration for all luminescence assays was 2 million cells/mL.

Biomaterials for Surface Zone

GelMA (58% methacrylated, 167kDa, Rousselot) and OMA were reconstituted in PBS containing 0.05% LAP (Cellink). Stocks were made my combining the material with PBS in Eppendorf tubes on a tube warmer at 50°C and shaken (800 rpm) until fully dissolved. To prepare biomaterial combinations, calculated amounts of each stock were added to Eppendorf tubes on the tube warmer at 50°C, with a quick vortex to fully combine. PBS containing 0.05%

LAP was added if further dilutions were necessary. All stocks and combinations were made less than 24 hours prior to use and stored in the dark at 4°C. To encapsulate cells, biomaterial combinations were warmed on the tube warmer to 37°C, cells added and vortexed to mix. The cell-biomaterial mixtures were either pipetted onto 96 well, white plates with a clear bottom for the DoE screen and subsequent validation or added to barrels (Nordson) for 3D bioprinting.

Design of Experiment (DoE) Trial Design

DoE for Middle-Deep Zone

An optimal combined design (Design-Expert Version 13, Stat-Ease) was determined with two mixture components: GelMA vol% and HAMA vol%, both 0-100%. Crosslinking time was a numeric factor, set as hard to change, ranging between 15 and 60 seconds. A quadratic-by-quadratic model with point exchange generated 18 total groups (Table 1). Groups were used for dynamic mechanical analysis as described below by casting disc constructs (8mm diameter x 1mm height) in silicone/glass molds. Following casting, the constructs were crosslinked as described below and then stored in Tyrode's in the dark at 4°C overnight. Storage moduli were analyzed using a linear regression model with no transformation to determine significant factors. DoE generated groups were also used in a screen with HuCOL2gLuc reporter cells, and the luminescence assay as described below. Analysis was completed using a linear regression model after a log base 10 transformation.

Table 1: Design of Experiment generated groups for middle-deep zone optimization

Number	**GelMA (vol)**	**HAMA (vol)**	**Crosslink (sec)**
1	0	1	15
2	1	1	15
3	1	0	15
4	0	1	38
5	0	1	38
6	1	1	38
7	1	0	38
8	1	1	38
9	1	0	38
10	1	2	38
11	1	1	38
12	2	1	38
13	0	1	60
14	1	1	60
15	1	1	60
16	1	0	60
17	1	3	60
18	3	1	60

DoE for Surface Zone

Stat-Ease, Design-Expert (Version 13) was used to generate testing conditions for screening combinations of GelMA and OMA at different photocrosslinking times. A mixture model was used in an optimal combined design generating a total of 60 conditions (Table 4). Constraints were set so the final percentage of GelMA in the mixture was between 0-12%, OMA was 0-2%, with the rest being PBS between 86-98%. The sum of the final percentages of GelMA and OMA was set to be between 2-14%, and the total sum of GelMA, OMA and PBS would always equal 100%. Crosslinking time was the numeric factor, ranging between 15-60s. To determine if the addition of calcium prior to cell encapsulation had an impact on lubricin expression, calcium inclusion was a categoric factor, resulting in groups with or without calcium (final concentration 1.8mM $CaCl_2$). DoE generated testing conditions were combined with HuPRG4gLuc cells and lubricin promoter-driven luciferase expression was assessed. Luminescence data was input into the DoE software where it suggested a square root model. After transformation of the data to fit the square root model, ANOVA analysis was used to identify the significance of the data.

3D Bioprinting

A BioAssemblyBot pneumatic extrusion 3D bioprinter (Advanced Solutions) was used to fabricate all 3D bioprinted constructs. Biomaterials were printed using disposable, UV-blocking amber cartridges (Nordson), SmoothFlow tapered tips (25G, Nordson) and a 35°C stage temperature and the print settings shown in Table 2 or 3. Tissue Structure Information Modeling (TSIM, Advanced Solutions) software was used to create 3D models. After printing, the constructs were photo-crosslinked (Luck Laser, 405nm, 300mW). The laser was focused to an

8mm beam diameter and positioned 3.5cm above the construct. Single layer prints were used for both cell viability and mobility to obtain clearer images, and more readily quantify cell numbers. For cell viability, 2mm x 6mm rectangular cuboids were printed in a single layer (~0.3mm height). For mobility, 6mm x 6mm rectangular cuboids were printed in a single layer (~0.3mm height, in three 2mm x 6mm sections, Fig. 6). Cylindrical constructs (8mm diameter x 1mm height) were printed containing HuCOL2gLuc cells for the luminescence assay and final mechanical characterization (the same dimensions used for DoE screen mechanical characterization).

Table 2: 3D Bioprinting settings for middle-deep zone biomaterials.

GelMA (15%):HAMA (2%) (vol:vol)	**Pressure (psi)**	**Acceleration (mm/sec^2)**	**Speed (mm/sec)**	**Ink Temp (ºC)**
1:1	15-13	200	5	25
2:1	21-18	200	7	28
3:1	22-17	200	7	28

Table 3: 3D Bioprinting settings for surface zone biomaterials

	Pressure (psi)	**Acceleration (mm/sec^2)**	**Speed (mm/sec)**	**Ink Temp (ºC)**
14% GelMA	16-14	100	9	24
14% GelMA, 2% OMA	33-18	100	5	25
16% GelMA	15-12	100	7	25

Mechanical Characterization

Dynamic Mechanical Analysis (DMA)

Before testing, discs were allowed to equilibrate to room temperature and the width and height measured with calipers (Netzsch). Unconfined uniaxial compression testing was performed (DMA 242E Artemis, Netzsch). Strain (10%, 100 μm) was tested at frequencies of 0.1, 1 and 5Hz. All tests were completed at isothermal (room) temperature and discs were maintained in Tyrode's for the duration of the test. Storage modulus (E'), loss modulus (E") and Tan delta were measured for 30 minutes, and final values were calculated from the average values between 5 and 10 minutes, during the curve plateau.

Lap-shear

Static coefficient of friction and kinetic coefficient of friction were determined through a lap shear test on disc constructs. Day 0 discs were cast in an 8mm diameter, 1mm high silicone mold, while day 22 constructs were 3D bioprinted discs of the same dimensions containing HuPRG4gLuc cells and cultured for 22 days. Constructs were frozen (-80°C) until use. Lap shear testing was preformed using a TA.XTplusC texture analyzer (Stable Micro Systems). The samples were adhered to a microscope slide (VWR) and placed securely into the top tensile clamp (Fig. 5). A second microscope slide was secured into the bottom tensile clamp. The sample was fully submerged in PBS for the duration of the test (Fig. 5). The sample was aligned until it was touching the second microscope slide and then compressed by ~200μm, creating a normal force of 1.62N. Normal force was determined by a force sensitive resistor (DF9-40, Yosoo Health Gear). The static force was determined by the peaks of the graph generated from a

shear sine wave test, while the kinetic force was determined from the slope. The coefficient of friction was calculated from the force generated on the graphs, divided by the normal force.

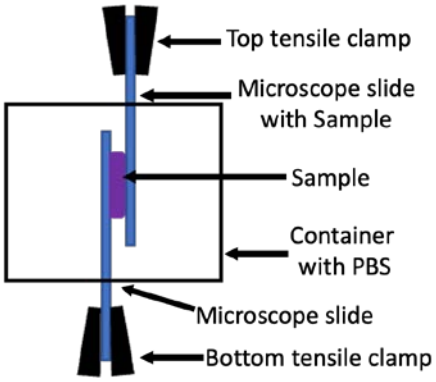

Figure 5: Lap-shear test set up on the texture analyzer

Luciferase Assessment

After correlation between luciferase expression and target genes was established, luciferase assessment was performed as a proxy to estimate type II collagen or lubricin expression in both the pipetted material DoE screen, and the 3D bioprinted discs. Constructs containing HuCOL2gLuc cells were cultured for 22 days in defined chondrogenic media with 1ng/mL TGFβ1 while constructs containing HuPRG4gLuc cells were cultured with 10ng/mL TGFβ1, with feeding every 2-3 days and sampling every 2 days to maintain a consistent timeframe (~48h). For this assay, conditioned cell culture media (20 µl/well) was transferred into a white 96-well plate (Greiner Bio-One) and mixed with a stabilized luciferase assay reaction mix (50µl) for final concentrations of 0.09 M MES, 0.15M Ascorbic Acid, and 4.2µM Coelenterazine. Luminescence was read on a plate reader (Biotek Synergy H1 Hybrid Reader or PerkinElmer EnVision 2104 Multilabel Reader).

Cell Viability

Live/Dead staining was used to evaluate the viability of human chondrocytes (1 million cells/mL final concentration) on days 0, 1 and 7. To quantify cell viability for the deep zone, uninfected human chondrocytes from the same donor, at the same passage, as the HuCOL2gLuc reporter cells and HuChon-GFP cells were used. GelMA (15% w/v):HAMA (2% w/v) volume ratios of 1:1, 2:1 and 3:1 were either 3D bioprinted, or pipetted (control) onto a BSA coated (3.15 mg/cm, Alfa Aesar) 24-well plate (Corning) and cultured in growth media. Plates were BSA coated to prevent cell adhesion. For the surface zone, HuPRG4gLuc cells passage 3 were used and groups 14% GelMA, 16% GelMA or 14% GelMA, 2% OMA were 3D bioprinted or pipetted (control). At each time point, media was removed and the staining solution of calcein-AM (2M, Invitrogen) in sterile PBS was added to each well. Samples were incubated for 25 minutes (37C, 5% CO_2). Imaging (4x magnification) was performed using a Pico Imager (Molecular Devices). Images were processed and analyzed using ImageJ/Fiji with the Stardist plugin [74], with >100 cells quantified for each sample.

Cell Mobility

HuChon-GFP cells were used to assess cell mobility. Three 2mm x 6mm sections were bioprinted forming one construct (Fig. 6, final 6mm x 6mm). The Cells section contained HuChon-GFP cells (1 million cells/mL final concentration) in GelMA (15% w/v):HAMA (2% w/v) mixtures at volume ratios of 1:1 or 2:1. The Spacer section was comprised only of biomaterial to act as a spacer between the cells and chemoattractant, printed with the same biomaterial volume ratio the cells were in. The final Chemoattractant section contained fibroblast

growth factor 2 (100ng/mL, basic FGF, Peprotech) in the 2:1 volume ratio. The chemoattractant was only added to the 2:1 ratio to eliminate any impact on diffusion rate by the material ratio. As a positive control for 2D cell mobility, cells were seeded directly to the 12-well plate (Corning). A separate control for directional mobility had all 3 bioprinted sections, except an extra spacer was bioprinted in place of where the chemoattractant was in the other groups. Three replicates were used for each group, and all constructs were cultured in growth media. Time lapse imaging was performed with a Pico Imager (Molecular Devices) at 4x magnification; images were captured every 20 minutes for 20 hours starting immediately after printing. Images were analyzed with ImageJ/Fiji (Version 2.3.0/1.53q) and the Manual Tracking plugin. For each well, all mobile cells were tracked, except for the positive control which had too many mobile cells to track, 7 randomly chosen cells were tracked. Tracked results included distance, velocity, and location (X, Y coordinates).

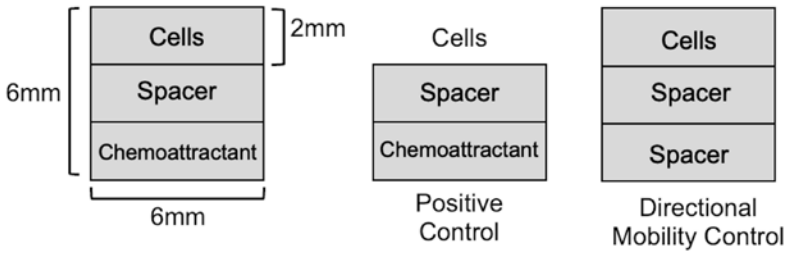

Figure 6: Experimental set up for chondrocyte mobility assessment

Biochemical Assays

Two thirds of the 8mm x 1mm bioprinted discs were frozen (-20°C) until the time of the assay. DNA, GAG and hydroxyproline (HDP) content were measured in samples from day 0 (immediately after printing) and day 22. Samples were digested overnight (65°C) in papain (0.025 mg/mL papain in 50mM sodium phosphate, 2mM EDTA, 2mM cysteine) [75,76]. DNA

content of the digest was measured using Hoechst dye (Ex365, Em460nm, SpectraMax iD5, Molecular Devices) with calf thymus DNA (Sigma) as a standard. GAG content of the digest was measured using the dimethyl methylene blue (DMMB) colorimetric assay [77]. DMMB working solution (5ml of 3.2mg/mL DMMB dissolved in 200 proof ethanol added to 1L of 40mM glycine, 40mM NaCl at pH 1.5) was added to each sample and absorbance was read at 525nm with correction at 595nm (SpectraMax iD5, Molecular Devices) with chondroitin sulfate (Seikagaku Biobusiness) as a standard [77]. For HDP, papain digested samples were acid hydrolyzed overnight (10:1 vol/vol, 6M HCL, 110°C) and then dried overnight (70°C). Copper sulfate (0.15M) and NaOH (2.5M) were added to each well and incubated (50°C, 5 minutes). Samples were oxidized through incubation with hydrogen peroxide (6% H_2O_2, 50°C, 10 minutes). Then sulfuric acid was added (1.5M H_2SO_4) before reaction with Ehrlich's reagent (10% w/v 4-dimethylamino benzaldehyde in 60% isopropanol, 26% perchloric acid, 14% MΩ water). Samples were incubated again (70°C, 16 minutes). Absorbance was read at 505nm (SpectraMax iD5, Molecular Devices) and total content was calculated using a hydroxyproline standard curve generated using hydroxyproline (Sigma). Samples of materials without cells were used to subtract background generated by gelatin. Data was then normalized to day 0.

Histology

At the end of the 22-day culture period, a third of the 8mm x 1mm disc was fixed in 10% Neutral Buffered Formalin (Epredia) for ~2 days. Samples were dehydrated and embedded in paraffin wax (Leica Biosystems Embedder). Rehydrated sections were stained with Safranin-O (0.02% Safranin O at pH 4.8 in water, Electron Microscopy Sciences) then counterstained with Fast

Green (0.05% solution fast green in 96.5% 200 proof EtOH and 3.5% Glacial acetic acid, VWR, Alfa Aesar) and Weigert's Iron hematoxylin (Electron Microscopy Sciences) for evaluation of sulfated GAG content. Immunohistochemistry was performed to evaluate type II collagen content. Pronase (1mg/mL in 5mM calcium chloride in PBS for 10 minutes at RT, Sigma) was used for antigen retrieval and tissue sections were blocked with BSA (3% w/v, Cohn Fraction V Alfa Aesar). The type II collagen primary antibody (1:200 in 1% BSA, DSHB, II-II6B3) was incubated for 2 hours at RT and the secondary antibody (1:200 in 1% BSA, Biotinylated horse anti-mouse, Vector Labs) was incubated for 1 hour at RT. Sections were then incubated for 30 minutes at RT with HRP-conjugated streptavidin (1:5000 in 1% BSA, Invitrogen), and staining was developed using Vector VIP Peroxidase Substrate Kit (VWR). For lubricin, hyaluronidase (10mg/mL in 20mM sodium acetate, Sigma) incubation at 37°C for 30 minutes was used for antigen retrieval. Samples were blocked with 3% BSA. Primary antibody (1:400, 1% BSA, Millipore MABT401) was incubated for 90 minutes at RT, and secondary antibody was incubated for 30 minutes at RT. HRP-streptavidin incubation and stain development was the same as for type II collagen. All sections were then counter stained with Fast Green (VWR). Images were taken using a Keyence BZ-X810 microscope.

Swelling and Degradation

3D bioprinted discs (8mm diameter x 1mm height) were frozen (-80°C) in weighed Eppendorf tubes (W_t), lyophilized and dry weights (W_i) were measured. Lyophilized discs were submerged in 1mL of chondrogenic media and incubated (37°C, 5% CO_2) for days 1, 11 and 22. Media was changed weekly. On days 1, 10 and 22 all media was removed, and swollen (W_s) weights were

measured. After weighing, samples were frozen (-80°C) and lyophilized again and weighed (W_d). To calculate the swelling ratio (Q) the swollen weight was divided by the initial weight ($Q = (W_s - W_t) / W_d - W_t$) [60]. The percent mass loss was calculated by $(((W_i - W_t) - (W_d - W_t)) / (W_i - W_t)) \times 100$ [60].

Lubricin (PRG4) ELISA

To quantify secreted lubricin, cell culture medium was collected from the TGFβ1 dose response on day 16 and from the 3D bioprinted disc constructs on days 1, 10 and 22. Cell culture medium was frozen at -20°C until use. Enzyme-Linked ImmunoSorbent Assay (ELISA) kit (DuoSet ELISA Ancillary Reagent Kit and Human Lubricin/PRG4 kit, R&D systems) was used following manufacturer's protocol. Lubricin content was calculated based on the standard curve.

Statistical Analysis

Design of Experiment analysis was completed as described previously using Design-Expert (Version 13, StatEase). All other experiments were performed with 3-9 replicates (n = 3-9). Quantitative results are shown as mean +/- standard deviation and statistical analyses were done using GraphPad Prism 9.0 or Design-Expert (Version 13, Stat-Ease). HuCOL2gLuc screen data was analyzed using ANOVA and Tukey's multiple comparison. Cell viability data was analyzed with a 2-way ANOVA and Sidak's multiple comparison for analysis of printed vs pipetted controls and Tukey's multiple comparison for comparing printed conditions over time. DNA, GAG, HDP and final storage modulus were analyzed with a 2-way ANOVA with Sidak's multiple comparison. The HuCOL2gLuc disc 3D bioprint and mobility were analyzed with an

unpaired t-test. A value of $p < 0.05$ was considered statistically significant. For the HuPRG4gLuc DoE screen, design of experiment analysis was completed as previously described. For all other HuPRG4gLuc experiments, statistical analysis was completed using GraphPad Prism (Version 9.0). All experiments had 3-9 replicates ($n = 3-9$) and results are shown +/- standard deviation. A p value of <0.05 was considered statistically significant.

CHAPTER 3: MIDDLE-DEEP ZONE ARTICULAR CARTILAGE

Overview

The hypothesis for this chapter was that an optimal biomaterial stiffness and/or combination of GelMA and HAMA is necessary to stimulate chondrogenesis, and therefore type II collagen production. To identify an ideal combination of GelMA and HAMA for chondrogenesis, a novel, primary human chondrocyte *COL2A1-Gaussia* luciferase reporter system (HuCOL2gLuc) was developed. With this non-destructive, high-throughput temporal assay, *Gaussia* luciferase is secreted from the cells and used as a proxy for measuring type II collagen production. GelMA:HAMA ratios were screened using the reporter system before proceeding to 3D bioprinting. This method is efficient, saving on time and materials, resulting in a streamlined process of biomaterial optimization. The screen revealed that the addition of HAMA to GelMA improved chondrogenesis over GelMA (15%) alone). Storage moduli were measured using dynamic mechanical analysis of the same GelMA:HAMA ratios and established an initial threshold for chondrogenesis of ~30kPa. To determine if biomaterial storage moduli impact cell mobility human primary chondrocytes transduced with green fluorescent protein (GFP) were 3D bioprinted in either 1:1 or 2:1 ratios with storage moduli of 32kPa and 57.9kPa, respectively. We found that reduced cell mobility, in the stiffer biomaterial had higher type II collagen expression, than the softer material with more cell mobility. Finally, after 3D bioprinting with HuCOL2gLuc cells we successfully identified an optimal combination (2:1) of GelMA:HAMA and photo-crosslinking time (38s) for chondrogenesis.

Stimulation of Type II Collagen by TGFβ1 in Primary Human Chondrocytes

TGFβ1 dose response was used to characterize the engineered primary human chondrocytes transduced with a type II collagen *Gaussia* luciferase construct (HuCOL2gLuc) derived from two donors. Dose dependent increases in luminescence are shown for day 8 (Fig. 7A) and day 17 (Fig. 7B). The excitatory concentration producing a half-maximal response (EC50) was calculated to be 0.780 ng/mL for day 8 and 2.702 ng/mL for day 17. Dose response curves for donor 2 had similar EC50 values of 0.142 ng/mL for day 7 (Fig. 26S) and 1.868 ng/mL for day 21 (Fig. 26S). Biochemical and histological analysis was performed on HuCOL2gLuc reporter cells to characterize their ability to produce extracellular matrix proteins. There was a TGFβ1 dose dependent increase of DNA (Fig. 26S), GAG (Fig. 7C), and GAG/DNA (Fig. 26S). Which was also supported by Safranin-O staining (Fig. 7F-H). HDP (Fig. 7D) and HDP/DNA (Fig. 26S) expression was consistent across groups. However, histology for type II collagen showed a TGFβ1 dose dependent increase in staining intensity (Fig. 7I-K). This data is consistent with the dose dependent increase in luminescence, indicating the HuCOL2gLuc reporter cells reflect type II collagen expression. This is further supported by qPCR analysis for *COL2A1* and gLuc. As *COL2A1* gene expression increased so did gLuc (Fig. 7E). Based on the maximal luminescence signal, donor 2 HuCOL2gLuc cells were used for all subsequent experiments.

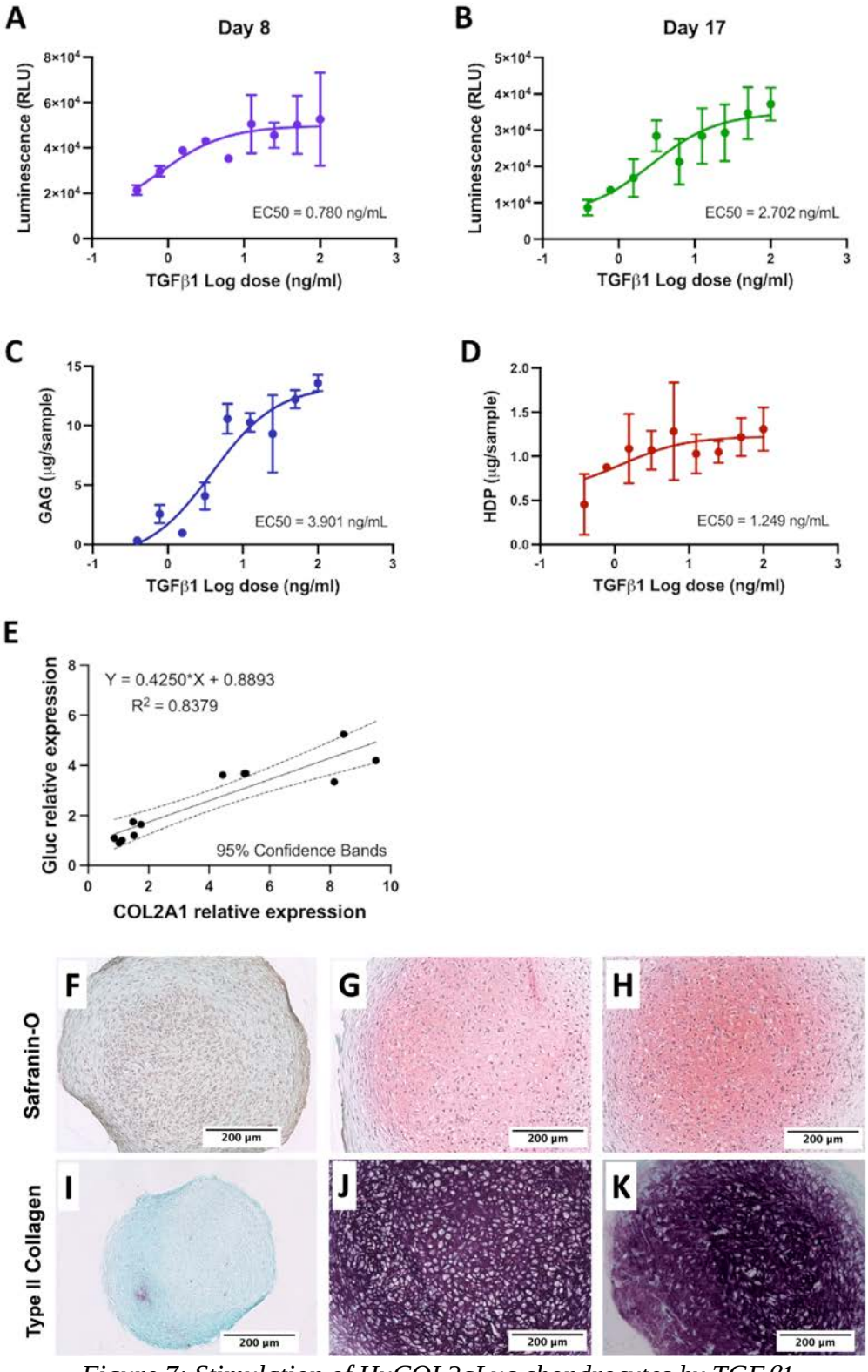

Figure 7: Stimulation of HuCOL2gLuc chondrocytes by TGFβ1

Initial Mechanical Characterization of GelMA:HAMA Constructs

Dynamic mechanical analysis (DMA) was used to measure the moduli (storage modulus (E'), loss modulus (E") and tan delta) of 18 different biomaterial ratios (GelMA:HAMA) after varying photocrosslinking times that were generated by the DoE software (Table 1). Storage moduli increased as the amount of GelMA increased and as crosslinking time increased (Fig. 8A). Three GelMA:HAMA ratios were too soft to be tested: 0:1 15s, 1:1 15s, and 1:3 60s. HAMA alone (0:1, at 38s and 60s) had the lowest storage moduli tested resulting in 6.9kPa and 11.9kPa, respectively. GelMA:HAMA 2:1 38s and 3:1 60s had the highest storage moduli tested at 57.9kPa and 60.6kPa, respectively. Residual data was normally distributed (Fig. 8B). It was found that the mixture of materials had a significant impact on the storage modulus (p=0.0006, ANOVA), but crosslinking time did not (p=0.0714, ANOVA). The opposite trend was observed for tan delta (Fig. 27S) in which shorter crosslinking time, and increased amount of HAMA increased tan delta. However, neither crosslinking time (p=0.2589) nor material mixture (p=0.1151) had a statistically significant impact. There were no trends observed for the loss moduli (Fig. 27S), and neither crosslinking time (p=0.9677) nor material mixture (p=0.3208) had a significant impact.

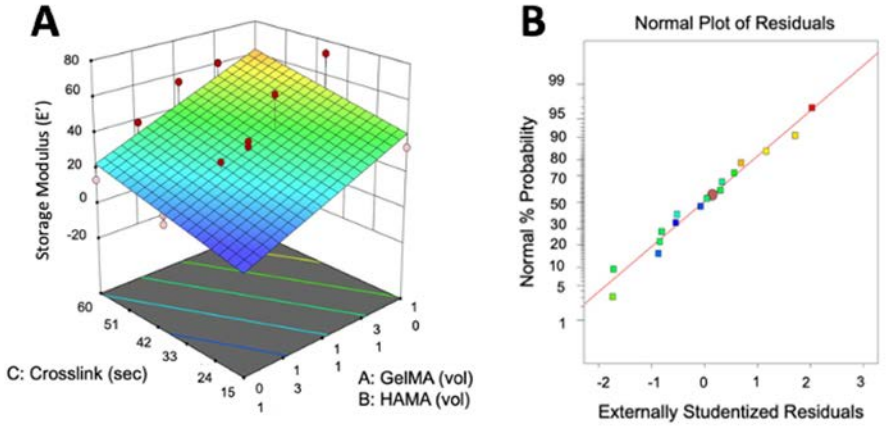

Figure 8: Storage moduli increases as GelMA content and crosslinking time increase

HuCOL2gLuc Screen of GelMA:HAMA Material Combinations

HuCOL2gLuc reporter cells were used to identify combinations of GelMA:HAMA that stimulated type II collagen expression. The combinations of GelMA:HAMA tested were generated by the DoE software (Table 1). These were the same 18 groups that underwent DMA assessment. Luminescence results for days 8 (Fig. 9A) and 22 (Fig. 9B) are shown with similar trends. HAMA alone (0:1) at all crosslinking times had significantly lower luminescence compared to all groups except 1:3 60s on day 8, and both 1:2 38s and 1:3 60s on day 22 (Fig. 9A and B). At the shortest crosslinking time (15s) luminescence was highest in GelMA alone (Fig. 9A and B). After 38s crosslinking the 2:1 ratio had the highest luminescence (Fig. 9A). Group 3:1 60s had significantly higher luminescence compared to GelMA alone on both days (Fig. 9A and B). Response surface analysis shows a clear peak in chondrogenic stimulation around the 3:1 ratio, at all crosslinking times (Fig. 9C). The normality plot (Fig. 9D) demonstrates the fit of the data and therefore the validity of the analysis used.

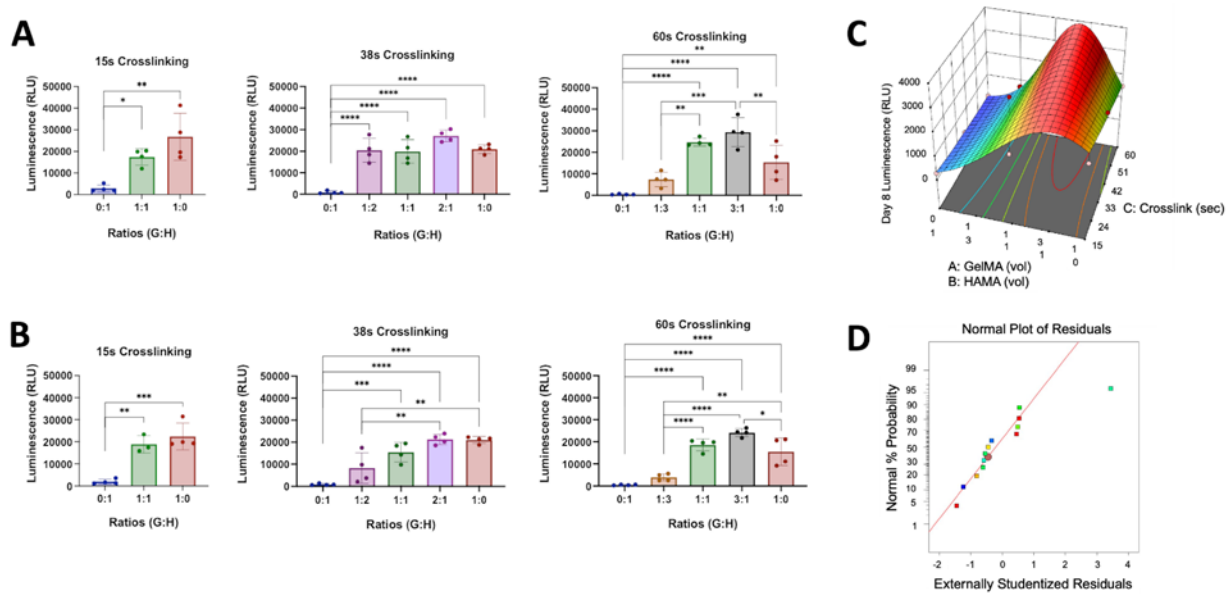

Figure 9: Biomaterial composition and storage moduli impact type II collagen production

To determine if biomaterials improved luminescence compared to traditional 3D cell aggregates, HuCOL2gLuc cells were seeded as aggregate cultures and luminescence assessed over 22 days. Temporal analysis of chondrogenic response showed an initial peak in luminescence on day 8 with an uptick at day 22 (Fig. 10A, 28S). All groups except 1:3 60s and HAMA alone after all crosslinking times had higher luminescence as compared to the cell aggregate control (Fig. 10A, 28S). However, when luminescence data is normalized to day 1 this trend changes (Fig. 29S). Groups 1:3 60s, and HAMA alone at 15s and 38s were similar to the cell aggregate control, while HAMA alone at 60s had higher luminescence (Fig. 29S). To analyze the impact of storage modulus on luminescence, cumulative luminescence vs. storage modulus was plotted (Fig. 10B). The softest materials tested, HAMA alone (0:1 38s and 60s) had the lowest level of luminescence. Above ~30kPa, there is a similar cumulative luminescence value for all groups (Fig. 10B).

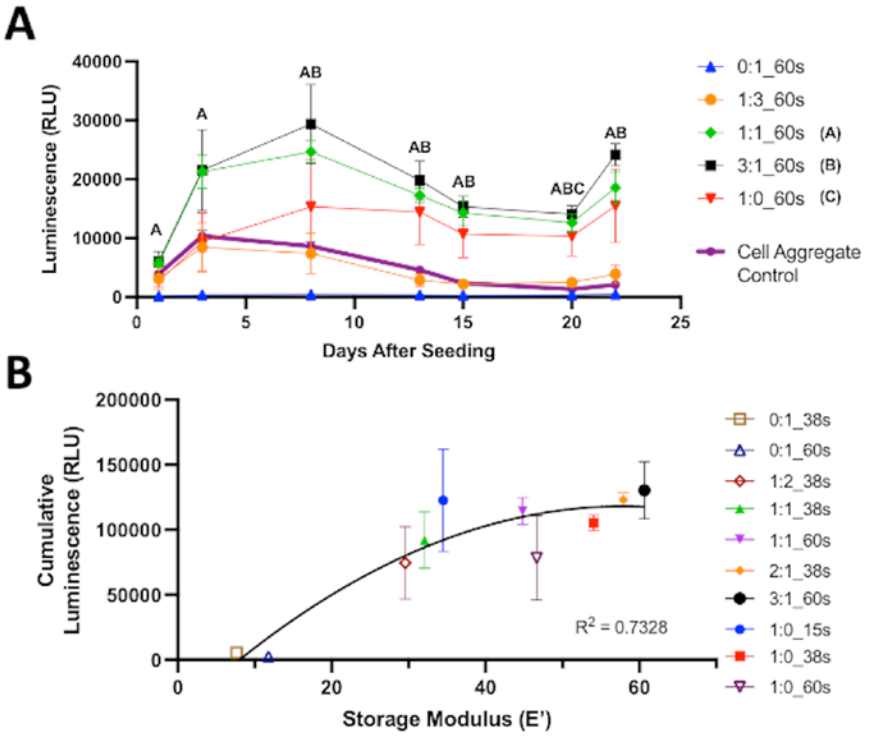

Figure 10: Type II collagen expression increases in biomaterials as compared to cell aggregates and storage modulus threshold for chondrogenesis

Human Chondrocyte Viability in 3D Bioprinted Constructs

GelMA:HAMA ratios of 1:1, 2:1 and 3:1 after 38s crosslinking were chosen for subsequent 3D bioprinting assays. To ensure the materials and 3D bioprinting process were biocompatible, cell viability was quantified on days 0, 1 and 7 (Fig. 11). As a control, the same biomaterial combinations were pipetted directly onto the plate. High cell viability was observed for all groups on all days, at 90% or higher (Fig. 11). On day 0 and day 1, viability was higher in the printed group at 1:1 (99%) than the pipetted (93-96%), this was also true for 2:1 on day 1 (100% for printed and ~96% for pipetted) (Fig. 11A). However, by day 7 all groups had similarly high percent viability (above 90%). To determine if cell viability changed over time, bioprinted material ratios were compared across all three time points (Fig. 11B). While the 1:1 and 3:1

groups remained consistent, the 2:1 group had a significant decrease by day 7 (~90%) as compared to day 0 (100%) and day 1 (99%). Representative images of all bioprinted groups on day 0 and day 7 are shown (Fig. 11C).

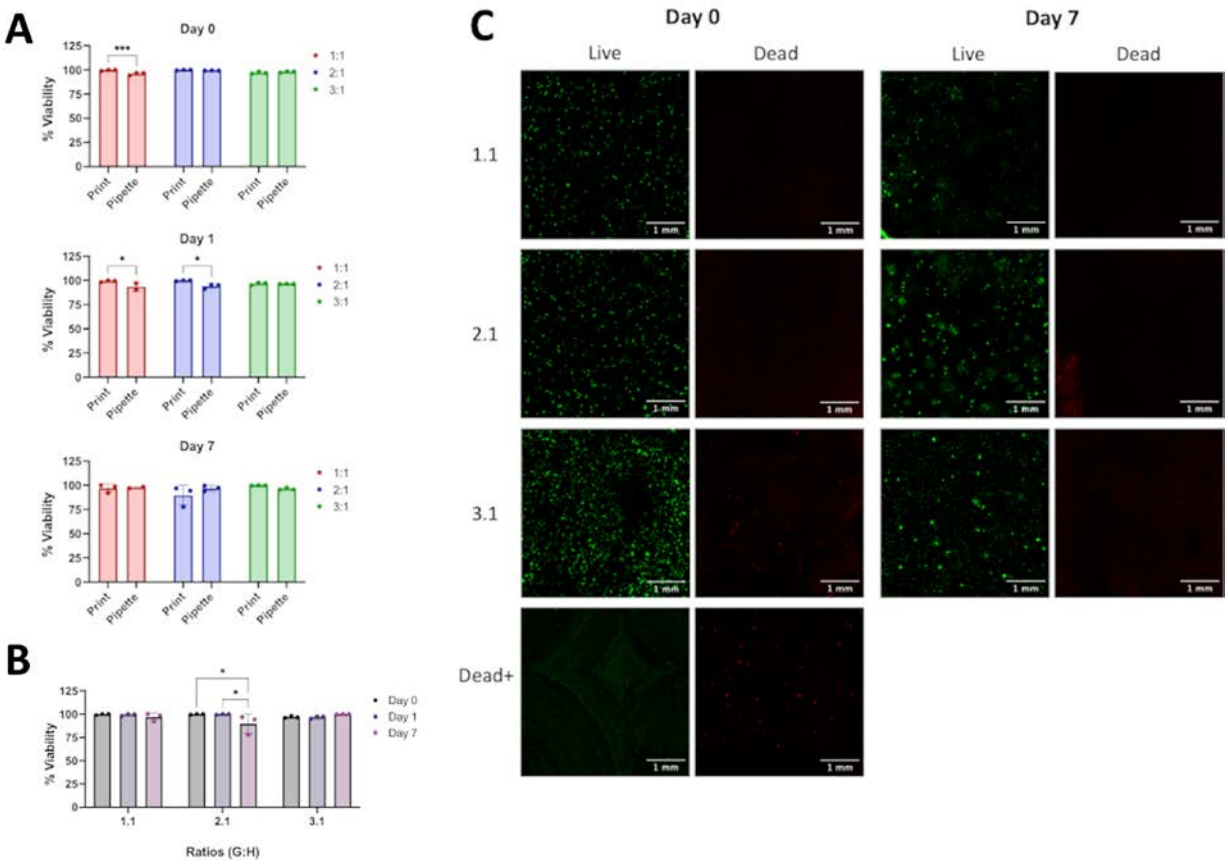

Figure 11: Primary human chondrocytes show high viability in 3D bioprinted constructs

Human Chondrocyte Mobility Within 3D Bioprinted Constructs

To determine the effect of biomaterial storage moduli on cell mobility, ratios of GelMA:HAMA ratios of 1:1 and 2:1 after 38s crosslinking were 3D bioprinted with HuChon-GFP cells encapsulated in the biomaterials. These ratios were chosen since 2:1 had a storage modulus of 57.9kPa, and 1:1 was roughly half at 32.0kPa. Expanded HuChon-GFP cells were fluorescent (Fig. 12E) and were readily visible within 3D bioprinted biomaterials (Fig. 12F). Timelapse

images over 20 hours showed that human primary chondrocytes are mobile in 2D in vitro culture, as demonstrated by the positive control (Fig 12A-C). In the biomaterials cells were minimally mobile, the 1:1 ratio had significantly more mobile cells (~2.5) compared to 2:1 (~1, Fig. 12A). Mobile cells also moved further (~26μm, Fig. 12B) and faster (~1μm/min, Fig. 12C) in the 1:1 ratio. Directionality of cell movement was also assessed and the 1:1 group had more variability in the movement (Fig. 12D). Overall, the softer material (1:1) had a higher level of cellular mobility as compared to the stiffer (2:1) material (Fig. 12).

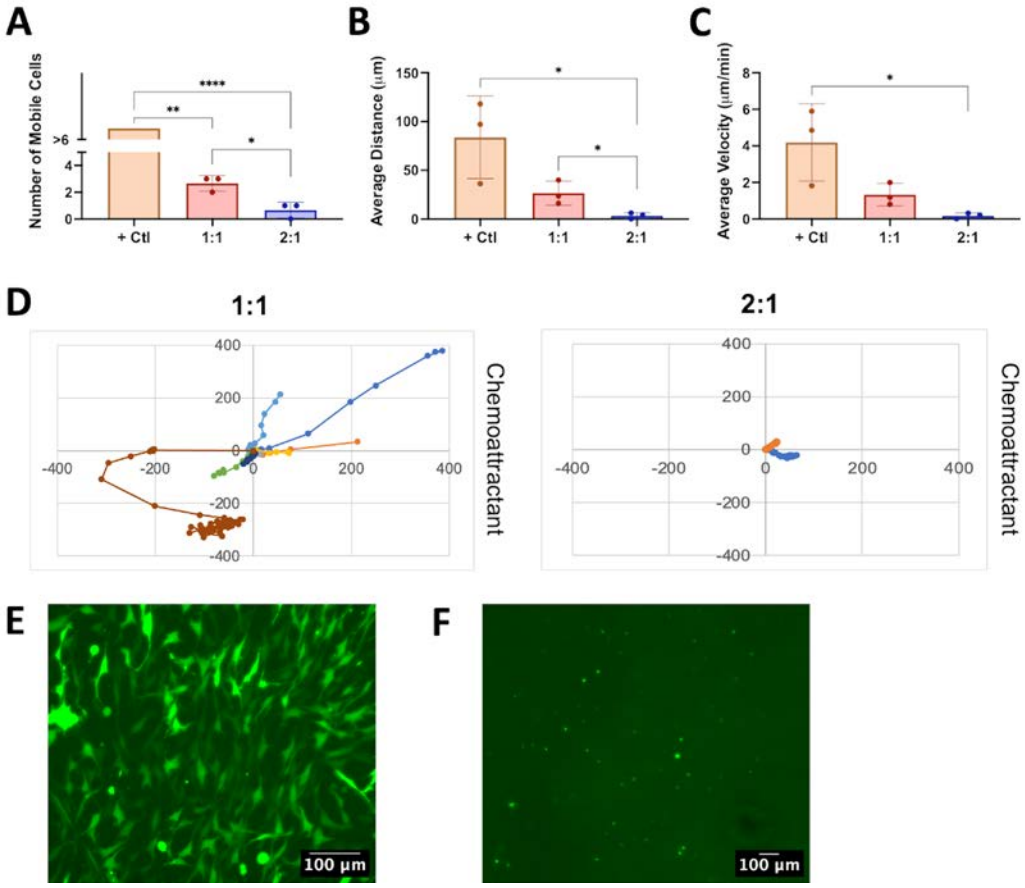

Figure 12: Human chondrocytes are less mobile in stiffer biomaterial

3D Bioprinted Discs Containing HuCOL2gLuc

Based on the luminescence and stiffness results generated from the HuCOL2gLuc DoE screen the 2:1 and 3:1 38s groups were chosen for 3D bioprinting. HuCOL2gLuc reporter cells were encapsulated in GelMA:HAMA ratios and bioprinted into discs then photo-crosslinked for 38s. To assess type II collagen expression, luminescence was measured over 22 days. Data was normalized to day 1 due to an initial difference in the raw luminescence data between the two groups (Fig. 30S). Luminescence peaked on day 3 (Fig. 13A, 30S). The 2:1 ratio had significantly higher luminescence at day 8 (~0.5 RLU) and day 22 (~0.4 RLU) when normalized to day 1 as compared to the 3:1 (Day 8 ~0.3 and day 22 ~0.2, Fig. 8B). Biochemical analyses were used to quantify the amount of DNA, GAG and HDP in the bioprinted constructs. DNA content was similar (1.3-2.3μg) between both groups at both time points (Fig. 14A). However, there was a significant increase in GAG production in the 2:1 group on day 22 (~7μg) as compared to day 0 (~2.5μg), while there was no increase in the 3:1 group (Fig. 14B). The 2:1 group also had significantly more GAG expression as compared to the 3:1 group on day 22 (~3μg, Fig. 14B). These trends were also observed in the ratio of GAG/DNA (Fig. 14C). Histology on day 22, for both GAG (Fig. 14E) and type II collagen (Fig. 14F) shows only minor staining, predominantly pericellular. The minimal staining is consistent with amount of staining observed in the cell aggregates at a similar TGFβ1 dose (Fig. 7F and 7I). There was a notable decrease in HDP of both groups from day 0 to day 22 (Fig. 14D). This correlated with a decrease in storage modulus from day 0 to day 22 in both groups (Fig. 15A), with a statistically significant decrease in the 2:1 group (~37 to 22 kPa). The storage modulus on day 0 increased with increasing frequency for both groups, but this increase was not observed on day 22 (Fig. 15B and

C). This trend was also observed in the complex modulus (Fig. 31S), loss modulus (Fig. 31S) and tan delta (Fig. 31S).

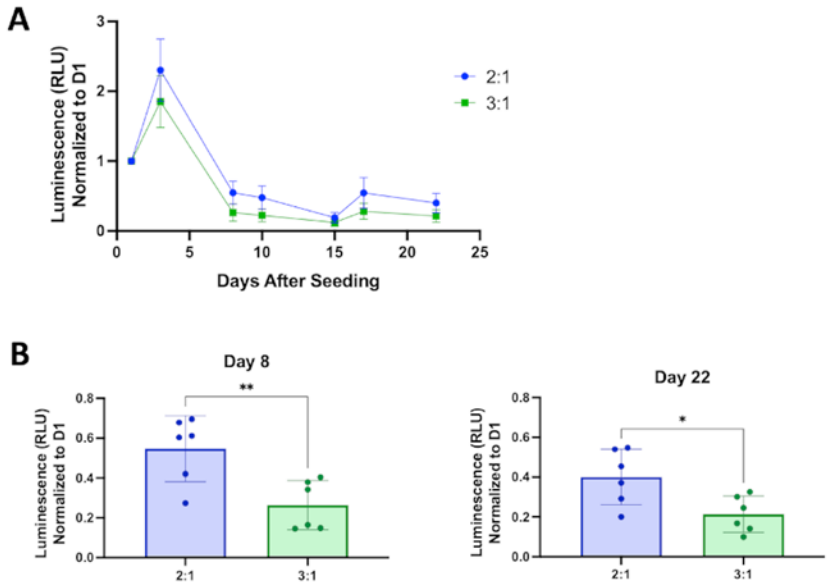

Figure 13: Luminescence is greater in GelMA:HAMA 2:1 bioprinted constructs

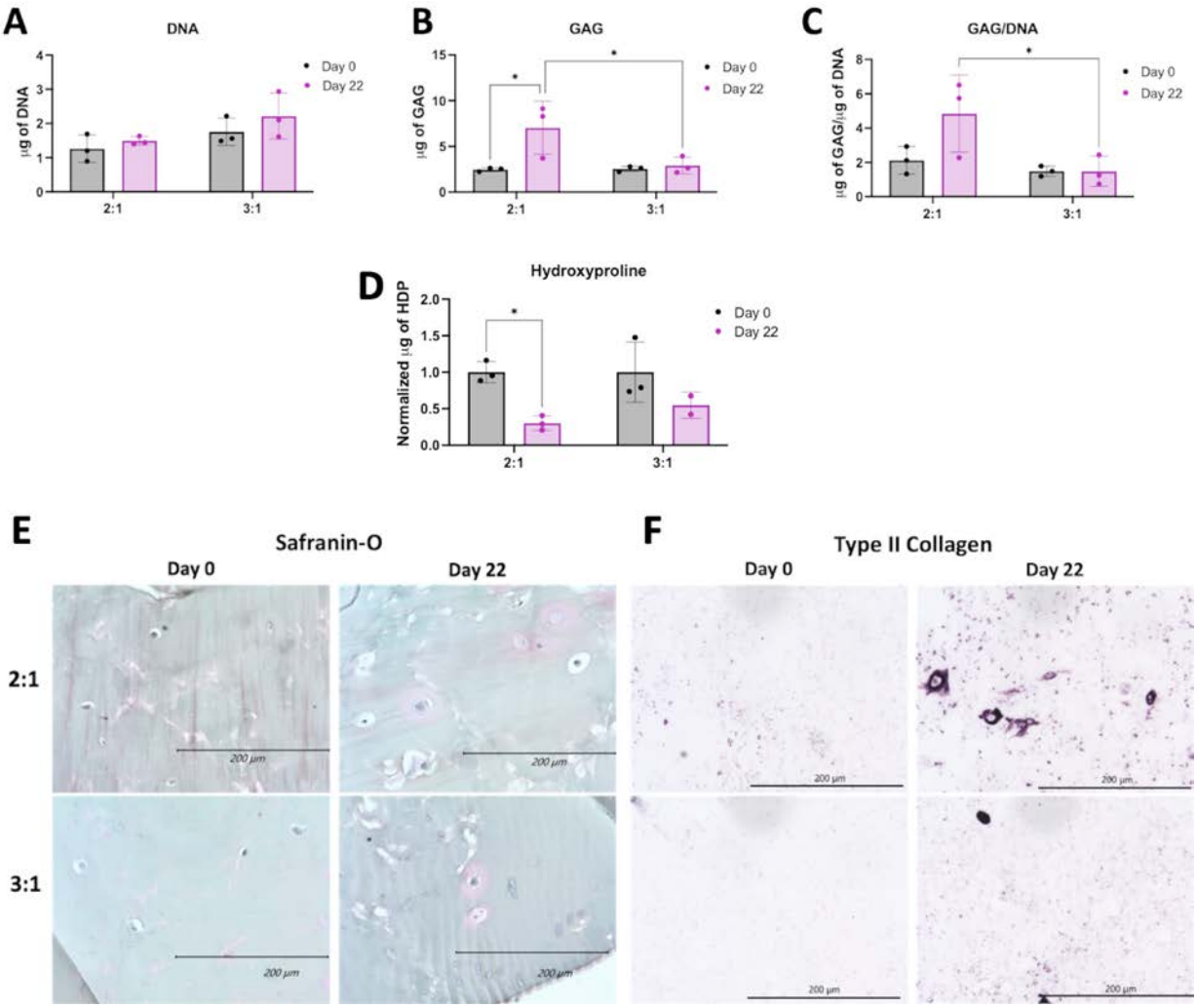

Figure 14: ECM deposition is greater in GelMA:HAMA 2:1 bioprinted constructs

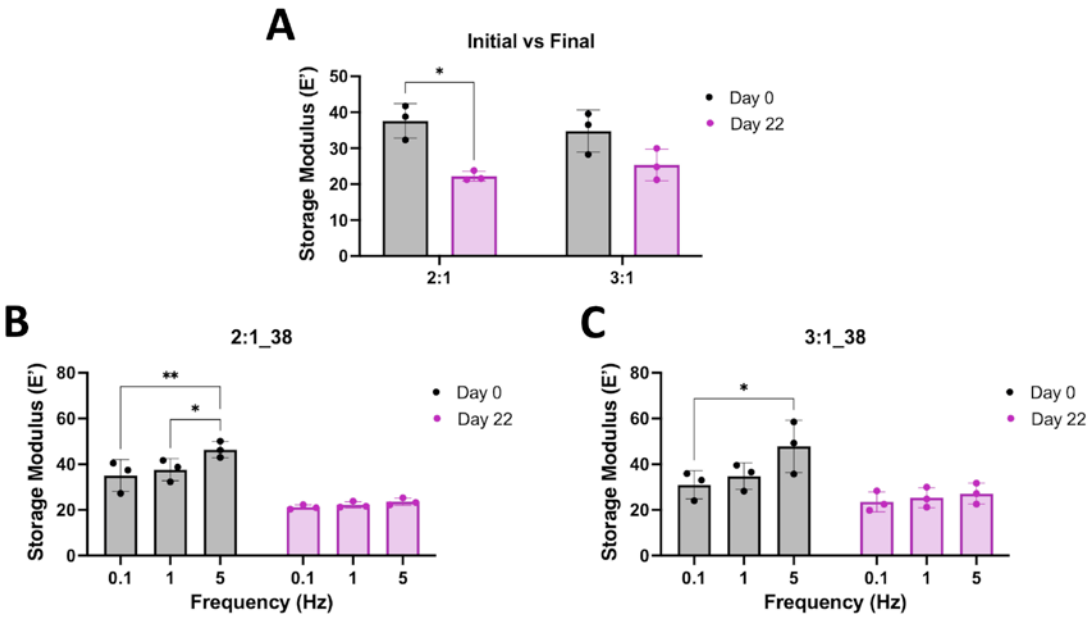

Figure 15: Storage moduli decrease from day 0 to day 22

CHAPTER 4: SURFACE ZONE ARTICULAR CARTILAGE

Overview

The hypothesis for this chapter was that an optimal combination of GelMA and OMA will improve lubricin expression, stiffness will modulate expression, and that combination can be optimized with human primary chondrocyte reporters. To test this, human chondrocytes were transduced with a *PRG4* (lubricin) promoter-driven *Gaussia* luciferase, allowing for temporal assessment of lubricin expression. A lubricin promoter-driven expression Design of Experiment screen and subsequent validation identified 14% GelMA/2% OMA as a combination for further study. Stiffness did not have a significant effect on lubricin expression in the range tested (E' 10-50KPa). This combination (14% GelMA/2% OMA) as well as 14% GelMA and 16% GelMA were 3D bioprinted. Lubricin expression (ELISA) and shape retention over the 22 days in culture determined the 14% GelMA/2%OMA to be the optimal combination.

Stimulation of Lubricin by TGFβ1 in Human Primary Chondrocytes

To characterize human primary articular chondrocytes engineered with a *PRG4* promotor driven *Gaussia* luciferase (HuPRG4gLuc), cell aggregates were cultured with varying doses of TGFβ1. Luminescence increased in a TGFβ1 dose dependent manner, as shown by the response curves for days 10 and 22 in Figure 16A. The excitatory concentration producing a half-maximal response (EC50) was 2.505 ng/mL on day 10 and 4.189 ng/mL on day 22 (Fig. 16A). Lubricin secretion also had a TGFβ1 dose dependent increase, with an EC50 of 4.260 ng/mL (Fig. 16B), very similar to the luminescence EC50. This is further supported by qPCR gene expression

analysis which correlated *PRG4* expression with gLuc gene expression (Fig. 16C). There was a TGFβ1 dose dependent increase of both DNA (EC50 = 2.764 ng/mL, Fig. 16D) and GAG/DNA (EC50 = 4.801 ng/mL, Fig. 16E), which is supported by Safranin-O staining (Fig. 17). While hydroxyproline (HDP) per DNA (Fig. 16F) was consistent across groups, immunohistochemical staining for type II collagen showed an increase in staining intensity with an increase in TGFβ1 (Fig. 17). Lubricin immunostaining showed an increase in staining intensity as TGFβ1 concentration increased (Fig. 17). Together these results support using luminescence as a proxy for lubricin expression, while confirming the engineered cells are still chondrogenic.

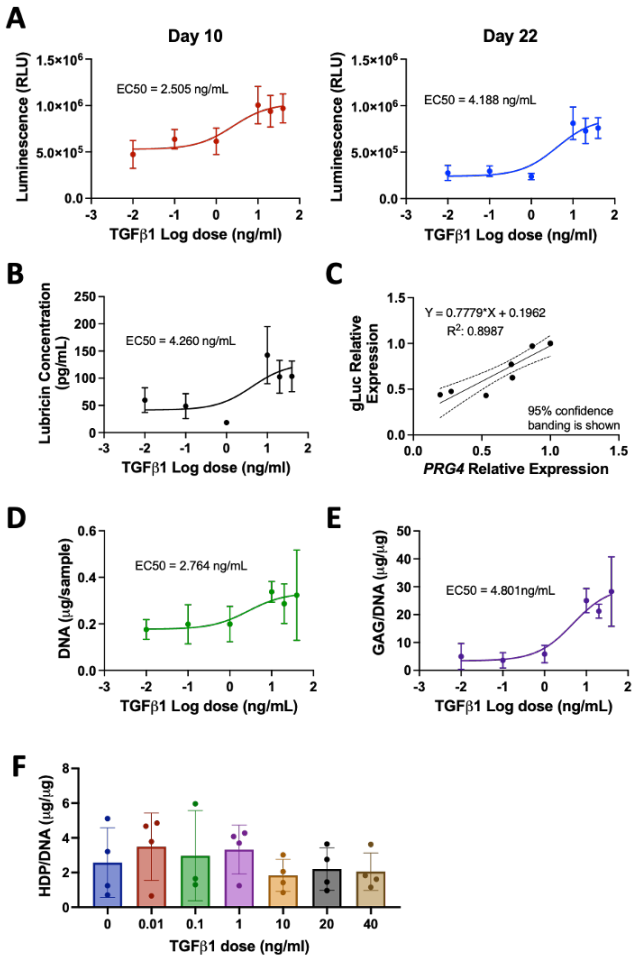

Figure 16: TGFβ1 stimulates lubricin expression

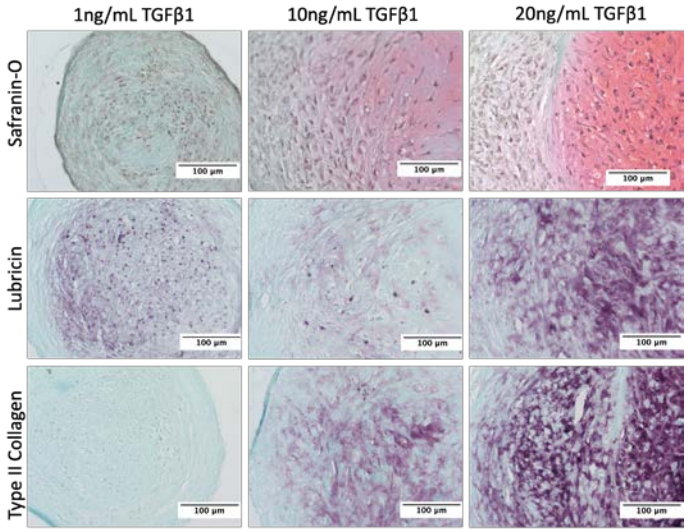

Figure 17: Histology staining of HuPRG4gLuc cell aggregates

DoE Screen of GelMA and OMA Combinations for Lubricin Expression

To identify optimal combinations of OMA and GelMA for lubricin expression, HuPRG4gLuc cells were mixed within biomaterial combinations generated by the DoE (Table 4). Sixty different combinations, at different crosslinking times, with or without the addition of calcium chloride were tested. At all timepoints the mixture of the biomaterials had a significant impact on luminescence ($p < 0.001$, ANOVA), while crosslinking time and calcium chloride were not significant factors. Day 22 luminescence is shown on 3D surface plots in Figure 4. Groups that contained only OMA had the lowest luminescence (Fig. 18A). Increasing GelMA to 6%, increased luminescence (Fig. 18B), with the shortest crosslinking time (15s) and no OMA having the highest luminescence. Luminescence further increased, by increasing GelMA to 12% (Fig. 18C). In the groups that had 12% GelMA (Fig. 18C), luminescence increased as the final percentage of OMA increased, with the highest luminescence expression in 12% GelMA/2% OMA. Data was normally distributed as shown in Figure 18D.

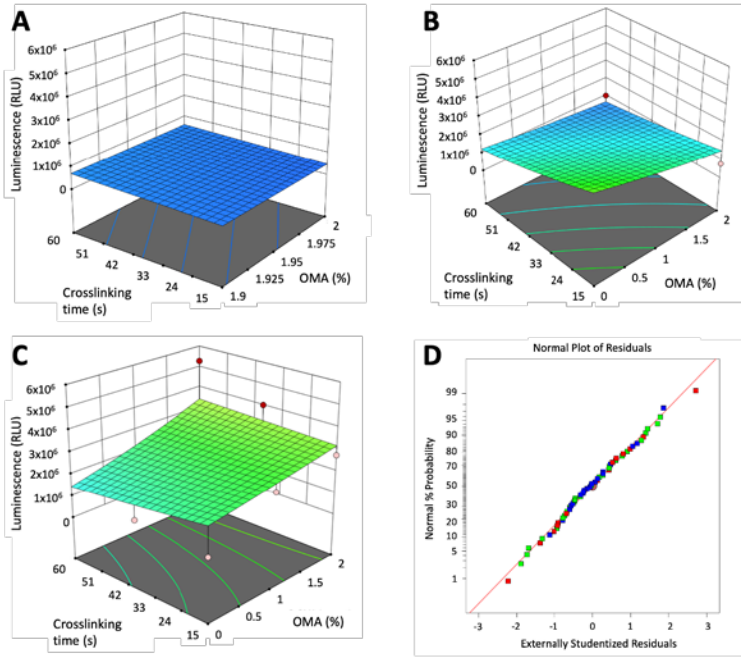

Figure 18: HuPRG4gLuc DoE screen day 22 results

Validation of the DoE Screen

Validation of the DoE screen results was performed using the HuPRG4gLuc cells cultured in combinations of GelMA and OMA. All biomaterial groups had higher luminescence than the cell aggregate control (Fig. 19A), indicating the mixing of chondrocytes in biomaterials increased lubricin expression. Day 22 luminescence data is shown in Figure 19. To validate the lack of effect of crosslinking time, the optimal group from the screen, 12% GelMA/2% OMA was retested at the three crosslinking times (15s, 38s and 60s). Crosslinking did not have a significant effect on luminescence (Fig. 19B). Since the highest final percentage of both GelMA and OMA had the highest luminescence in the screen, both were further increased, and luminescence was assessed. Increasing the final OMA percentage to 4% did not significantly impact luminescence at either crosslinking time (Fig. 19C). Increasing the final GelMA percentage to 14%, while

keeping OMA consistent at 2% did significantly increase luminescence as compared to 12% GelMA/2% OMA at both crosslinking times (Fig. 19D). To determine if this increase in luminescence was solely due to increasing the GelMA percentage, 14% GelMA alone was compared to 14% GelMA/2% OMA at both crosslinking times (Fig. 19E). The group containing 2% OMA had significantly higher luminescence as compared to 14% GelMA alone at 15s crosslinking, but not 38s (Fig. 19E). The 14% GelMA/2% OMA group after 15s crosslinking was consistently the group with the highest luminescence starting on day 10 (Fig. 19A). DNA content stayed consistent across all 14% GelMA groups (Fig. 32S), but GAG/DNA was significantly higher in 14% GelMA/2% OMA group at both crosslinking times (Fig. 32S). Based on the luminescence, DNA and GAG data the 14% GelMA/2% OMA at 15s was determined optimal for lubricin expression.

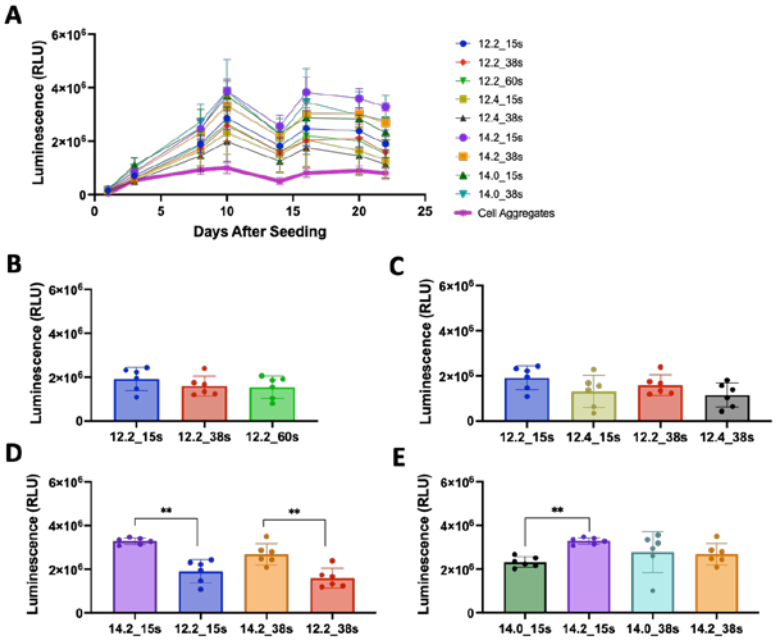

Figure 19: 14% GelMA/2% OMA had the highest lubricin expression

Cell Viability

Cell viability was assessed in groups 14% GelMA/2% OMA, 14% GelMA and 16% GelMA to ensure the bioprinting process and biomaterials were biocompatible. Groups were either 3D bioprinted or pipetted and viability was quantified on days 0, 1 and 7. On days 0 and 1 cell viability was significantly decreased in all 3D bioprinted groups, as compared to their respective pipetted controls (Fig. 33S). By day 7, the 14% GelMA and 16% GelMA printed groups still have significantly lower cell viability as compared to their pipetted controls, but the 14% GelMA/2% OMA printed group was significantly higher than the pipetted (Fig. 33S). On day 0, the 16% GelMA printed group had the lowest viability at only 54%, but it significantly increased to 72% by day 7 (Fig. 20). The 14% GelMA printed group cell viability significantly decreased over 7 days from 77% to 61% (Fig. 20). Finally, the 14% GelMA/2% OMA group stayed consistent across all 7 days at around 72% viability (Fig. 20).

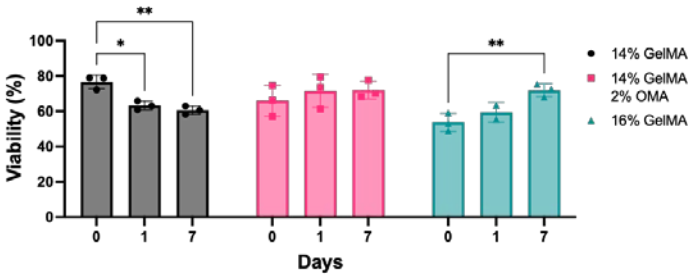

Figure 20: Cell viability results for 3D bioprinted HuPRG4gLuc cells

3D Bioprinted Disc Construct Containing HuPRG4gLuc Cells

The 14% GelMA/2% OMA after 15s crosslinking had the highest luminescence in the validation, and improved GAG deposition, therefore it was used for 3D bioprinting disc constructs

containing HuPRG4gLuc cells. As controls 14% GelMA and 16% GelMA with 15s crosslinking were also printed into discs. Luminescence was assessed over 22 days (Fig. 21). The 16% GelMA group had significantly higher luminescence starting on day 3 as compared to the other two groups (Fig. 21A). Day 10 and Day 22 have the same trend with 16% GelMA having significantly higher luminescence, and no difference between the 14% GelMA/2% OMA and 14% GelMA groups (Fig. 21B).

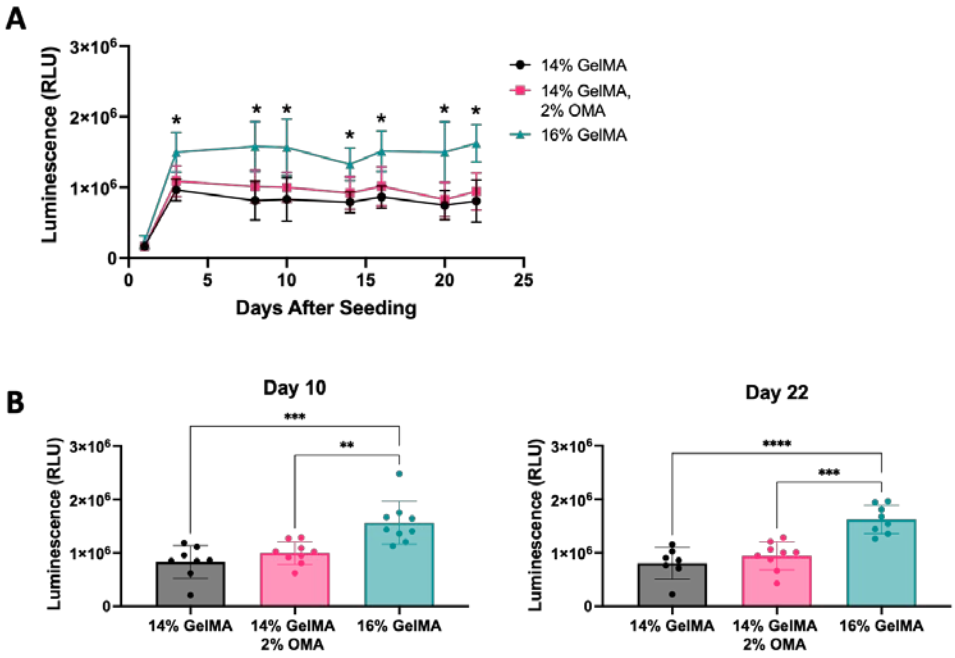

Figure 21: 16% GelMA had the highest luminescence in 3D bioprinted disc constructs

DNA and GAG content were quantified from constructs on day 0 and day 22. DNA content stayed consistent in both 14% and 16% GelMA, but the 14% GelMA/2% OMA had a significant increase by day 22, as well as having significantly more DNA than both the 14% and 16% GelMA groups on day 22 (Fig. 22A). The 14% GelMA/2% OMA and 16% GelMA had a significant increase in GAG by day 22, while 14% GelMA did not (Fig. 22B). The 14% GelMA/2% OMA on day 22 had significantly more GAG than both other groups (Fig. 22B).

GAG/DNA significantly increased for all three groups by day 22 and the 14% GelMA/2% OMA had significantly more GAG/DNA than the 14% GelMA group (Fig. 22C), which was consistent with the GAG/DNA from the validation (Fig. 32S).

Secreted lubricin content was quantified by ELISA from culture media on days 1, 10 and 22. Lubricin concentration increased from day 1 to day 10, reflecting the luminescence results (Fig. 22D). On day 10, 14% GelMA/2% OMA and 16% GelMA had significantly more lubricin than the 14% GelMA group (Fig. 22D). On day 22, the 14% GelMA/2% OMA and 16% GelMA groups still had significantly more lubricin than the 14% GelMA group, but 14% GelMA/2% OMA also had significantly more than 16% GelMA (Fig. 22D). The 16% GelMA group had a significant decrease in secreted lubricin content from day 10 to day 22 (Fig. 22D).

Lubricin content retained in the biomaterials and type II collagen content was assessed by immunohistochemistry (Fig. 22E). The 16% GelMA group had more lubricin staining than either other group, while 14% GelMA had very minimal staining (Fig. 22E). The 14% GelMA group also had less type II collagen staining (Fig. 22E). The type II collagen staining in 16% GelMA was darker, but more pericellular as compared to the 14% GelMA/2% OMA group where it is lighter but more spread out (Fig. 22E).

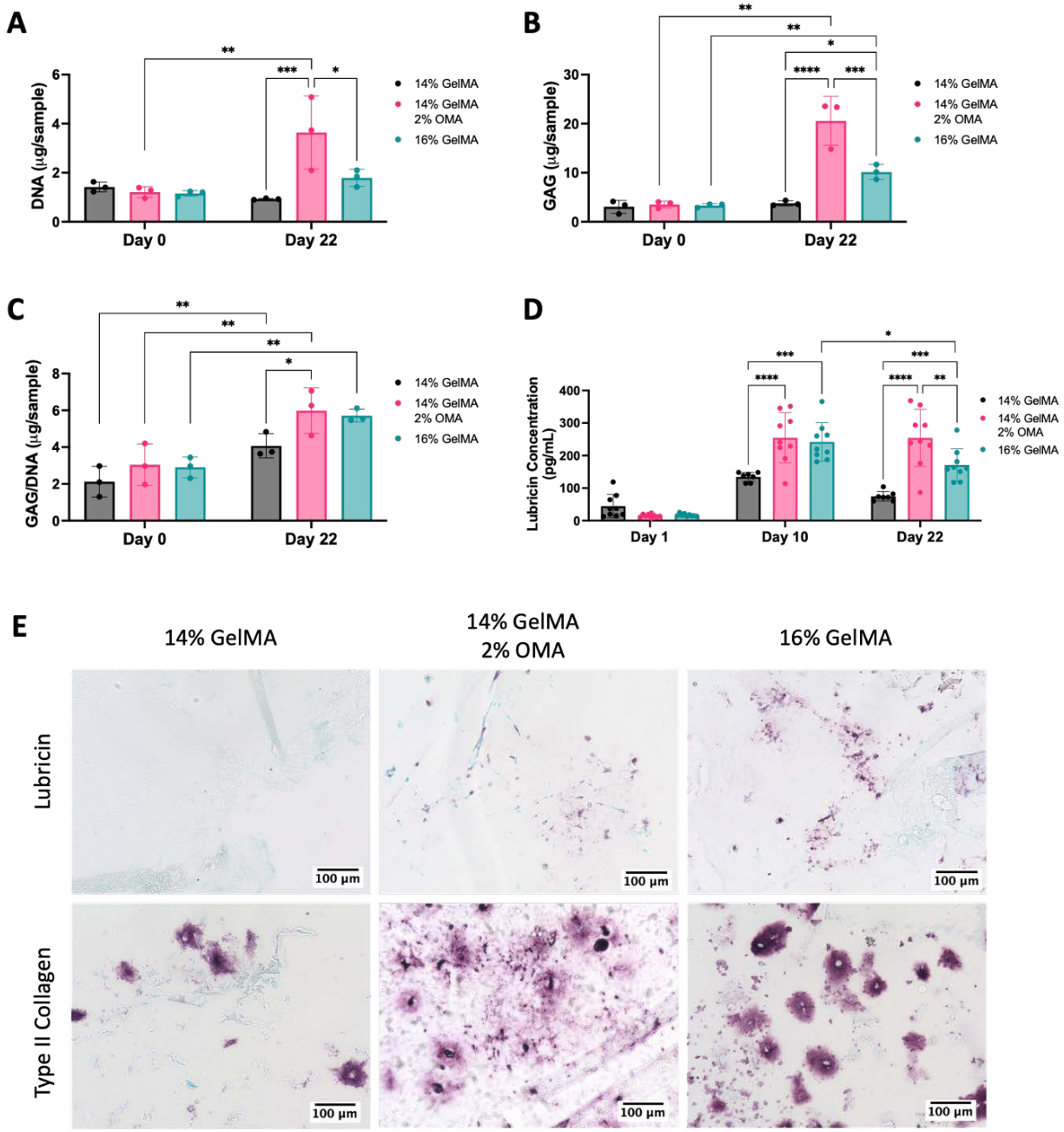

Figure 22: Biochemical results for 3D bioprinted disc constructs

Mechanical Characterization of Disc Constructs

To determine if hydrogel mechanical properties had an impact on lubricin expression, discs were cast and tested on a dynamic mechanic analyzer (DMA). The moduli generated were plotted vs cumulative luminescence from the validation. There was no trend for either storage modulus or loss modulus (Fig. 34S) with the R^2 values being 0.2670 and 0.1319, respectively. This data indicates these mechanical properties of the biomaterials tested, generated by DMA, play a minimal role in lubricin expression.

DMA analysis was also carried out to characterize 3D bioprinted discs containing HuPRG4gLuc cells on day 0 and 22 for biomaterials after 15s crosslinking. On day 0, both 14% GelMA and 14% GelMA/2% OMA had a storage modulus of ~30kPa (Fig. 23A). The storage modulus for 16% GelMA storage modulus was significantly higher than the other groups at ~60kPa (Fig. 23A). By day 22, the 14% GelMA group had decreased in size too much to be reliably tested. The 16% GelMA storage modulus significantly decreased by day 22 to ~24kPa (Fig. 23A). While the 14% GelMA/2% OMA storage modulus decreased to ~12kPa, but this change was not statistically significant (Fig. 23A). These trends are consistent for the loss modulus, tan delta, and complex modulus (Fig. 35S).

Lap shear testing was completed on both day 0 and day 22 constructs to determine the coefficient of friction. For both the kinetic (Fig. 23B) and static (Fig. 23C) coefficient of friction on day 0, there was no significant difference between the groups. As with the DMA testing, 14% GelMA was too small and thin by day 22 to be reliably tested. By day 22, both the 14% GelMA/2%

OMA and 16% GelMA groups had a significant decrease in the static (Fig. 23C) and kinetic (Fig. 23B) coefficient of friction to ~0.03. There was a significant difference in the static coefficient of friction on day 22 between the 14% GelMA/2% OMA (0.01) and 16% GelMA groups (0.005, Fig. 23C).

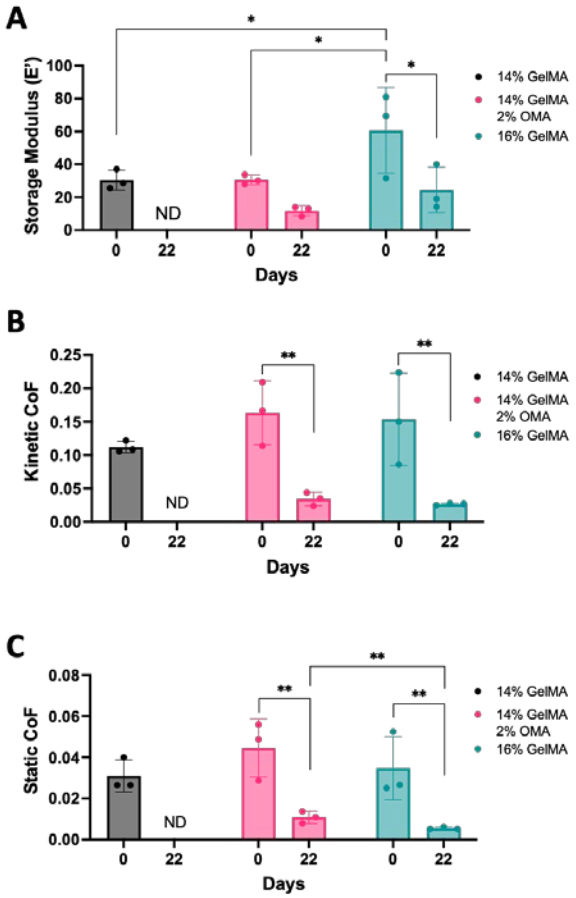

Figure 23: Storage modulus and coefficient of friction decrease over 22 days

Shape Fidelity of the Bioprinted Constructs

Over the course of the 22 days in culture, the 14% and 16% GelMA groups noticeably decreased in size, while the 14% GelMA/2% OMA retained its shape. To quantify the size, images were taken on day 22 (Fig. 24A) and the surface area was measured. Both 14% and 16% GelMA had a

significantly smaller surface area as compared to the 14% GelMA/2% OMA group (Fig. 24B). Yet, the swelling ratio stayed consistent for all groups over the 22 days (Fig. 24C). All constructs loss about ~12% of their mass on day 1 and ~25% by day 22 (Fig. 24D). No group lost significantly more than either other group at any time point.

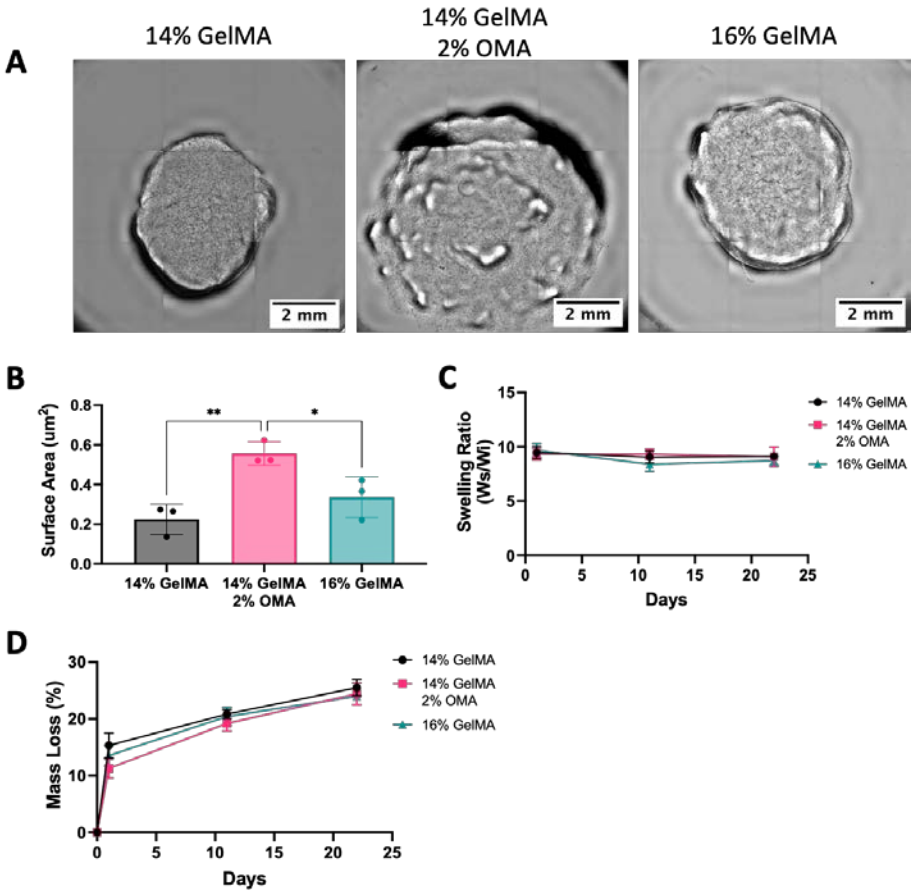

Figure 24: GelMA only groups decrease in size over 22 days

CHAPTER 5: DISCUSSION

Defects to articular cartilage often result in osteoarthritis (OA). While OA has traditionally been thought of as a disease of the elderly, the incidence of post traumatic OA (PTOA) is most common in younger individuals [6]. Unfortunately, there are limited treatment options for younger patients. A potential solution is 3D bioprinting. 3D bioprinting can be used to fabricate a cartilage construct that mimics the zonal architecture of native tissue, stimulating repair of the defect site. However, one challenge of 3D bioprinting is biomaterial selection and optimization. There are many 3D bioprinting materials available and while their material and biocompatibility characteristics such as printability and cell viability are well established, we sought to take a more biological phenotype outcome-based approach and characterize the articular chondrocyte extracellular matrix response. By using our novel human articular chondrocyte reporter cells, we were able to determine the chondrogenic response to biomaterials. We identified an optimal biomaterial combination for both the middle-deep and surface zones of articular cartilage based on ECM driven luminescence, mechanical properties, shape fidelity, and biochemical assays.

Reporter Chondrocyte Characterization

This dissertation presents the first examples of primary human articular chondrocytes as phenotypic reporter cells. This was achieved by improvements in isolation, preservation, and transduction of primary human chondrocytes. Previously, ATDC5s were transduced with a type II collagen promoter-driven *Gaussia* luciferase and used for micronutrient optimization of chondrogenic media [22]. A secreted *Gaussia* luciferase reporter enables a non-destructive temporal assessment of type II collagen or lubricin expression over 22 days through conditioned

media assessment at feedings. Type II collagen was used as a proxy for middle-deep zone chondrogenesis since it is both the main component of articular cartilage, and it is difficult to achieve native levels of expression *in vitro* [21]. Lubricin was investigated as it is an essential proteoglycan for articular cartilage function and treatment with lubricin mimetics have been shown to reduce the damage of PTOA in rats [33–35].

A TGFβ1 dose response was used to characterize reporter cells in cell aggregate culture and to confirm they retained their chondrogenic capacity after the transfection process. TGFβ1 is a known stimulator of type II collagen [18,78–81] and lubricin [18,28,82] expression. TGFβ1 binds to a serine threonine-protein kinase receptor consisting of two type I (ALK5) and two type II (TGFβRII) subunits (Fig. 25) [28,79]. This stimulates the phosphorylation of the Smad2 and 3 which then forms a complex with Smad4 (Fig. 25) [28,79]. This complex translocates into the nucleus and activates transcription of target chondrogenic genes [28,79].

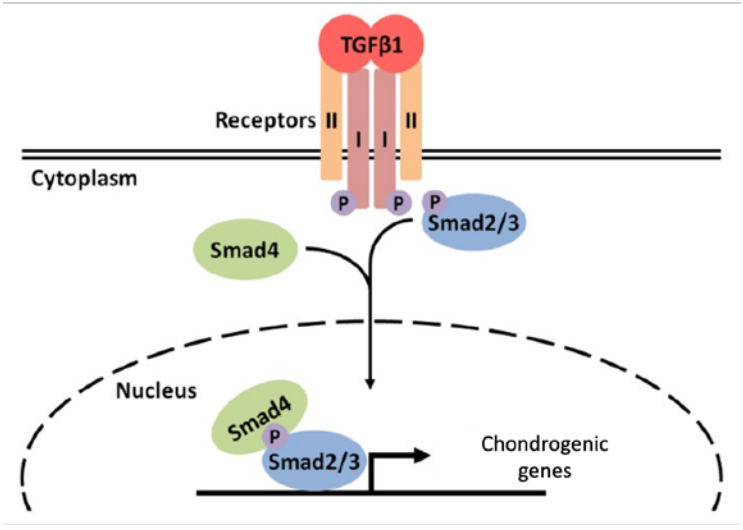

Figure 25: TGFβ1 signaling pathway (Adapted from [79])

HuCOL2gLuc and HuPRG4gLuc reporter cells both showed a TGFβ1 dose dependent increase in luminescence. This luminescence correlated with either type II collagen or lubricin expression through qPCR gene expression analysis, immunohistology staining and ELISA for lubricin. Quantification of the DNA content of the aggregates allows us to determine if the changes in luminescence are due to an increase in cell number or a reflection of the cells actually producing more type II collagen. Determining the GAG content and safranin-O staining confirm the production of GAG and homogenic chondrogenic capacity of the cells in the biomaterials. While GAG production is not as difficult *in vitro* as type II collagen, we do not want to increase type II collagen production at a detriment to GAG production. Together these results support using luminescence as a proxy for type II collagen or lubricin expression, while also confirming the genetically engineered cells are still chondrogenic. Chondrogenicity is a concern when using a primary chondrocyte where population doublings are a limiting factor [72,73,83].

Streamlining Biomaterial Optimization

For the first time, we demonstrate the advantages of using human primary phenotypic reporter cells for biomaterial optimization. This approach was successfully used to measure type II collagen [22] and lubricin expression within biomaterials. This study was further enabled by using a DoE approach. The DoE software generates test conditions using statistical modeling to reduce the number of conditions tested, while still having a good overview of the design space. A mixture design approach is an established [67–69] and efficient method to investigate how biomaterial properties are affected by altering the composition and crosslinking times. Since 3D bioprinting is a laborious process and utilizes significant amounts of biomaterials, reporter cells

were mixed within DoE generated groups, pipetted onto a 96 well plate and then crosslinked. The luminescence data produced from the screen was analyzed using the DoE software to further define optimal conditions. The combination of the reporter cells and DoE creates an efficient method to optimize biomaterial combinations and crosslinking time before proceeding to 3D bioprinting. To test all of the DoE generated groups without the reporter cells would use a significant amount of materials and cells. For perspective, to 3D bioprint the 12 replicates in the GelMA/OMA disc bioprinting 850µl of biomaterials per group was used and a total of $1.1x10^7$ cells between all three groups. Three replicates were saved for day 0 histology, biochemical and mechanical assessment, but the other 9 were cultured for the 22 days. The alternative would be to have specific time points and rely solely on end-point assays. To have a minimum of 6 replicates (3 for histology/biochemistry, and 3 for mechanical) for 4 time points (ex. days 0, 1, 11 and 22) about 1.7mL of biomaterials and $2.2x10^7$ cells would be used, double what was used in this dissertation. That is only for the 3 groups used for the 3D bioprinting, it would be significantly more if all 60 groups from the DoE were not screened prior to bioprinting. That method also only produces results for 4 time points, while the reporter cells are assessed for luminescence at about 10 time points. It also does not include the amount of biomaterials used to determine the print settings (~1.5mL of each combination). It is unrealistic to 3D bioprint with all of the DoE generated groups, but that means optimal combinations may be missed or left untested.

Optimized GelMA:HAMA Ratio for Middle-Deep Zone Articular Cartilage

GelMA and HAMA were chosen as the biomaterials for this study since their individual material characteristics are well established, both are commercially available and widely used in cartilage

tissue engineering [43]. Several studies have combined the two for 3D bioprinting of cartilage [84–93] to investigate numerous concepts including sterilization techniques [86], cell density and patterning [85], cell types [89], and printing techniques [84]. The significance of our work is this is the first study to determine an optimal ratio of GelMA and HAMA for type II collagen expression in human cartilage 3D bioprinting.

Storage Modulus Threshold for Chondrogenesis

Articular cartilage functionality is dictated by its mechanical properties therefore, it is unsurprising that assessment of these properties in biomaterial constructs is a significant area of research [43]. However, mechanical testing of constructs is most often performed prior to encapsulation of cells and without 3D bioprinting [43]. A few studies have compared mechanical properties from day 0 vs. end point to demonstrate how matrix deposition increases mechanical stiffness [94–96]. Those studies present initial stiffness as a baseline to improve upon, instead of a necessary characteristic of the biomaterials. One study has determined the minimal initial stiffness required for chondrogenesis to be 7-33kPa of chondroitin sulfate containing hydrogels with a mixture of adipose derived stem cells and neonatal calf chondrocytes encapsulated [97]. Another study determined ~30kPa Young's modulus to be ideal for human articular chondrocytes embedded in silk/fibrin hydrogels [98]. Due to the variety and inconsistencies in mechanical testing however, it is difficult to make comparisons between studies [99], and as such it has yet to be determined conclusively what initial storage modulus is required for chondrogenesis. Our results confirmed that a storage modulus threshold of ~30kPa needs to be reached to promote middle-deep zone chondrogenesis. Storage moduli were significantly

affected by the mixture of GelMA:HAMA. Importantly, the HuCOL2gLuc reporter cells provided a rapid and easy method to identify correlations between type II collagen expression and biomaterial mechanical properties.

GelMA:HAMA Stimulation of Type II Collagen

Using HuCOL2gLuc reporter cells we assessed type II collagen expression via luminescence in DoE generated material ratios. Previous studies showed poor cell spreading and adhesion in HAMA [56,57], we postulate this as an explanation for the low type II collagen expression in the predominantly HAMA groups. Interestingly, the addition of HAMA to GelMA improved type II collagen expression over GelMA alone at the same crosslinking times. This is likely due to hyaluronic acid providing biochemical cues and being a GAG present in native cartilage tissue [54] in combination with the cell adhesion sites found in gelatin [50,51].

Hyaluronic acid predominantly binds to the CD44 receptor on chondrocytes [54,100–102]. Activation of this receptor has been shown to be involved in a variety of intracellular signaling pathways including the internalization of hyaluronic acid, cell migration, proliferation, and adhesion to ECM components [100]. Hyaluronic acid has also been shown to stimulate TGFβ mRNA expression [101]. It has been postulated that hyaluronic acid stimulated synthesis of ECM components is through induction of TGFβ or through an autocrine signaling mechanism [101]. The side chains of hyaluronic acid are capable of binding multiple receptors at once [100]. It is unclear if gelatin is capable of stimulating type II collagen, other than GelMA being used so frequently for cartilage 3D bioprinting, but that could simply be due to its ease of use.

However, as previously stated gelatin is a hydrolysis product of collagen which also contains sites for MMP degradation [50,51]. Chondrocytes do secrete MMPs [103], so it is possible the degraded gelatin provides the amino acids used to generate type II collagen.

However, there was a complex interplay between biomaterial composition, storage moduli and photocrosslinking on chondrogenesis. GelMA alone after 15s photocrosslinking had similar luminescence to the 2:1 38s and 3:1 60s, despite a storage modulus of ~35kPa as compared to ~60kPa in the 2:1 38s and 3:1 60s mixtures. This has important implications for the field as there are a significant number of biomaterials currently available, along with different crosslinking methods, whose use in combination has not yet been studied. Using the high-throughput method described in this dissertation to screen material combinations can streamline the process and help save on time and materials.

Cell Mobility in GelMA:HAMA

Cell mobility was used to further characterize the cell response to the biomaterials. Native chondrocytes are generally considered to be relatively immobile due to the dense ECM, one of the reasons believed to cause the limited healing capacity of cartilage [104] Yet cell mobility is a hallmark of tissue remodeling and repair. It could be expected that, with chondrocyte ECM production and remodeling of the 3D bioprinted materials, cell mobility would increase. Mobility has been shown *in vitro* both in 2D with bovine chondrocytes [10,11] or ATDC5s [12] and 3D culture with bovine [13] rabbit [14,15] chondrocytes. But what about cells embedded in a 3D

printed bioink? To our knowledge, this is the first study measuring primary human chondrocyte cell mobility within a 3D bioprinted cartilage construct. We assessed cell mobility for the first 20 hours after 3D bioprinting in either 2:1 or 1:1 ratio of GelMA:HAMA after 38s crosslinking. These ratios were chosen to further understand the role of storage moduli on cell mobility as the storage moduli of 1:1 was about half that of 2:1. Perhaps unsurprisingly, our results showed the material with the higher storage modulus had significantly less cell mobility. Critically, the 2:1 ratio was one of the ratios with the highest type II collagen expression. This implies that chondrocytes favor an environment that restricts cell movement for chondrogenesis, particularly type II collagen expression, potentially because it is a closer mimic to native cartilage.

It should be noted however, that only a very small fraction of the total cells in the constructs, regardless of the material ratios, demonstrated mobility. It is possible that some cell movement was missed because of the difficulties in imaging a 3D construct, like imaging the full depth of field with clarity. This could also be because of the short time frame the cells were imaged. We only assessed mobility for the first 20 hours after bioprinting, and it is likely there was a lag period in cell movement and growth. It is possible that later time points would have a higher number of mobile cells as they produce more ECM and remodel the biomaterials.

3D Bioprinted GelMA:HAMA

Disc constructs were 3D bioprinted with the HuCOL2gLuc reporter cells. GelMA:HAMA ratio of 2:1 with 38s photocrosslinking was chosen because it had one of the highest storage moduli tested and was among the highest cumulative luminescence in the screen. While 3:1 with 38s

crosslinking was chosen because there was a trend of luminescence increasing in the GelMA only group as crosslinking time decreased. Since 3:1 has a higher ratio of GelMA than 2:1 it was expected that the luminescence would increase if the crosslinking time was decreased from 60s to 38s. This also maintained a consistent crosslinking time between groups. Both groups had a cell viability of above 90% at all time points, which is above the 70% threshold required to have a successful implant [105]. We therefore identified the 2:1 ratio as having the best chondrogenic response.

Strikingly, despite good luminescence over the 22 days for both groups, storage moduli decreased by day 22 as compared to day 0. This trend was also observed with the complex moduli, loss moduli and tan delta. All moduli on day 0 increased with increased frequency, however by day 22 they stayed consistent across all frequencies, indicative of a loss or reduction of viscoelasticity. Based on the frequency dependent storage moduli on day 0 the materials were more viscoelastic, but the constructs lost this property by day 22 [106]. This observation is likely due to an imbalance of ECM production and material degradation i.e., the chondrocytes degraded the material faster than they produced ECM. There are several factors that likely contributed to these results: 1) The slower rate of ECM production could be due to a decreased chondrogenic capacity of the cells. While we showed that the HuCOL2gLuc reporter cells maintained their chondrogenic capacity, it should be noted that, the chondrocytes used were sourced from elderly patients undergoing a total joint replacement. However, the type of cells used in this study could be either a cell source or the target population for treatment of osteoarthritis, therefore it is important to assess biomaterial effect on these cells. 2) Cell density could be an explanation for the decrease in storage moduli. In this study, the final cell density was 2 million cells/mL. This

density was chosen for the DoE screen to achieve a total of 50,000 cells/well, the same number used to seed cell aggregates, and was maintained for consistency in the subsequent 3D bioprinting. While this is a lower cell density than often reported in the literature, it is still within range for 3D bioprinting with human articular chondrocytes [107–109]. 3) The low TGFβ1 concentration (1ng/mL) used in the chondrogenic media. Low TGFβ1 was chosen for this study so any stimulatory effects of the biomaterials, including through the TGFβ1 pathway, would be evident and can be attributed to the biomaterials, not masked by a maximal stimulus produced by higher levels of TGFβ1. As such ECM production rate was reduced. 4) The initial threshold for chondrogenesis might be higher than we determined. Our results showed that an initial storage modulus of ~30kPa was necessary for chondrogenesis but ~60kPa was the highest storage modulus determined, only double our determined threshold. It is possible that by increasing the initial storage modulus, material degradation and ECM production may be reduced or prevented. 5) Degradation of the bioink reduced the stiffness of the material to levels below the threshold, resulting in reduced chondrogenicity during the 22-day culture.

However, if the goal is to increase the compressive stiffness of the biomaterials over the 22-days, optimizing for aggrecan expression would likely be more advantageous over type II collagen expression. Much of the compressive strength of articular cartilage comes from the proteoglycan content and therefore water retention [8,110]. The GAG chain on proteoglycans cause osmotic swelling within the tissue, when pressure or load is present on the joint the fluid flows out, but once the load is removed it flows back in [8]. It has been shown the compressive stiffness increases with increasing GAG content, while no specific correlation has been made with collagen content [110]. However, since these molecules form a specific interconnecting network

within cartilage this is likely more complicated and results from an interplay of the two with the GAG/collagen ratio being important in tissue engineered cartilage [21,75].

Deep Zone Optimization Conclusions

This study successfully identified an optimal combination of GelMA and HAMA for middle-deep zone chondrogenesis using HuCOL2gLuc phenotypic reporter cell type II collagen expression, biomaterial storage moduli and cell mobility. The HuCOL2gLuc reporter cells provided fresh insight on the storage modulus threshold required for chondrogenesis by correlating type II collagen expression with storage modulus of the same biomaterials. It was also determined that there is less chondrocyte mobility in the stiffer biomaterials and that reduced mobility correlated with increased chondrogenesis. Together these results indicate that a composite biomaterial with a higher storage modulus and less cell mobility, improved chondrogenesis.

A limitation of this study was using the biomaterials as a ratio, instead of working in final percentages within the DoE software. This meant that the only percentage of GelMA tested without the addition of HAMA was 15% w/v and the only percentage of HAMA tested without GelMA was 2% w/v. The 2:1 ratio had a 10% w/v GelMA and ~0.66% w/v HAMA, but those final percentages were never tested individually. It could be that diluting GelMA down to 10% is what improved luminescence and not the addition of HAMA, and without testing 10% GelMA that is unknown. It is unlikely, given the positive qualities of HAMA, but this oversight was remedied in the optimization for the surface zone.

Optimization of GelMA and OMA for Surface Zone Articular Cartilage

For the surface zone cartilage, we used gelatin methacrylate (GelMA) and oxidized methacrylated alginate (OMA). GelMA is a commonly used biomaterial for 3D bioprinting of cartilage [49,84–88,95,96,111–120], used in about 35% of cartilage 3D bioprinting papers since 2012 [43]. While GelMA has advantageous properties, we sought to control the degradation rate and study its chondrogenic capacity when mixed with OMA. Alginate is another frequently used biomaterial, but has the distinct drawback of not being naturally degradable in humans [60] nor having any cell adhesion sites [121]. One method to accelerate the degradation rate of alginate is oxidation, making it more vulnerable to hydrolysis [60]. To further create a biomaterial with tunable degradation rates, oxidized alginate was methacrylated adding a secondary location for hydrolytic degradation [60]. Previously, OMA containing human bone marrow-derived mesenchymal stromal cells has been 3D bioprinted in complex geometries with high resolution and high cell viability [61]. Our study is the first-time mixtures of GelMA and OMA were 3D bioprinted with primary human articular chondrocytes. Previously, we hypothesized that an imbalance in ECM production and material degradation rate contributed to a decrease in material storage modulus overtime [122]. By combining GelMA and OMA we hypothesized this would improve the stability of the construct, while still providing the biochemical cues necessary for lubricin expression.

GelMA/OMA Stimulation of Lubricin

To determine which combination of GelMA and OMA was beneficial for lubricin expression, an initial DoE screen was performed. Groups that were OMA alone had the lowest luminescence. Since OMA is chemically modified alginate it has no cell binding motifs and is not a component of ECM like HAMA or GelMA. These results showed that OMA alone does not stimulate lubricin expression, but with the addition of GelMA, lubricin expression increased. The highest final percentage of GelMA and OMA in the screen, 12% and 2% respectively, had the highest lubricin expression. Therefore, in subsequent studies, the final percentages were further increased. It was found that increasing the final percentage of OMA from 2% to 4% (with 12% GelMA) was not beneficial for lubricin expression, however increasing GelMA from 12% to 14% was. In the screen 12% GelMA/2% OMA had higher lubricin expression as compared to 12% GelMA alone, and in the validation 14% GelMA/2% OMA had higher lubricin expression as compared to 14% GelMA alone in the final week. This indicates that while increasing GelMA to a higher percentage increased lubricin expression, the addition of OMA was still beneficial. This could be because OMA is acting to stabilize construct and allowing for continual lubricin expression for the full 22 days, while the GelMA alone had faster degradation and limited lubricin expression in the final week.

Interestingly, unlike with type II collagen expression, storage modulus had no impact on lubricin expression. When storage modulus was plotted vs. cumulative lubricin luminescence there was no correlation between the two. This could be because lubricin does not play a role in

contributing to the structural stiffness of articular cartilage, unlike type II collagen. Or it could be that we were not within the storage modulus range to determine this impact.

3D Bioprinted GelMA/OMA

Based on the luminescence and GAG/DNA results of the validation, the 14% GelMA/2% OMA after 15s crosslinking was chosen for subsequent bioprinting. While 14% GelMA and 16% GelMA (also 15s crosslinking) were also 3D bioprinted as controls either for the effect of GelMA alone or for the total hydrogel content respectively. Luminescence data showed that increasing the final GelMA percentage increased the lubricin expression, since the 16% GelMA group had the highest luminescence. However, 14% GelMA/2% OMA secreted more lubricin from the construct as shown by ELISA, while the 16% GelMA group retained more within the construct as shown by immunohistochemistry. This is consistent with lap-shear data that showed the 16% GelMA group had a significantly lower static coefficient of friction as compared to 14% GelMA/2% OMA. More lubricin was still present in the 16% GelMA construct effectively reducing the coefficient of friction. This could be because lubricin has been shown to adsorb to type II collagen [123]. While lubricin was shown to adsorb to three types of collagen surfaces: denatured, amorphous and fibrillar, and therefore binding did not depend on the molecular or supramolecular structure of collagen [123]. It is possible that lubricin was able to bind more readily to the 16% GelMA because had a higher concentration of gelatin, a hydrolysis product of collagen.

The lubricin immunohistochemical staining was rather sparse overall, and this could be due to lubricin also being secreted. It could also be due to the cell density within the construct. The cell density was kept consistent from the screen through the bioprinting, originally chosen to compare between the cell aggregate control and the biomaterials. However, the surface zone of articular cartilage has a cell density at about 150 million cells/cm^3 of adult cartilage tissue [124], and mimicking that *in vitro* may increase lubricin expression. It should also be noted that the chondrocytes used in this study were a mixed population, not exclusively surface zone chondrocytes. It has been shown that even with TGFβ stimulation, middle and deep zone chondrocytes had barely any lubricin expression [28]. Incorporating solely surface zone chondrocytes may result in higher and more evenly distributed lubricin expression.

3D Bioprinted Construct Shape Fidelity

One of the requirements for an ideal tissue engineered articular cartilage construct is it needs to not only fill the defect space but maintain that space while new tissue forms [40]. Meaning that the 3D bioprinted construct must retain its shape while forming cartilage tissue. All 3D bioprinted groups lost about 25% of their mass over the course of 22 days in chondrogenic media, without cells present. However, when bioprinted with articular chondrocytes encapsulated there was a noticeable decrease in size in both the 14% and 16% GelMA groups, while the 14% GelMA/2% OMA group retained its shape. Both the 14% and 16% GelMA groups had a significantly smaller surface area by day 22 as compared to 14% GelMA/2% OMA. This could be because 14% GelMA/2% OMA had a higher GAG content by day 22 and the type II collagen appeared more dispersed throughout the construct. This stabilizing effect is likely

because of the presence of OMA and its controllable degradation rate. It is possible that by adding 2% OMA to 16% GelMA we could see more lubricin secretion and construct stabilization over the 22 days, however higher final percentages of biomaterials increases the difficulty in handling/bioprinting. Finding the balance between biomaterial degradation and tissue formation will continue to be a challenge in tissue engineering, but biomaterials like OMA can facilitate finding that equilibrium.

Surface Zone Optimization Conclusions

This study successfully determined an optimal combination of GelMA and OMA for lubricin expression supporting surface zone articular cartilage 3D bioprinting using our novel HuPRG4gLuc reporter cell system. Combining DoE with the HuPRG4gLuc cells created a more streamlined and systematic approach to test biomaterials for 3D bioprinting. While the 16% GelMA group had the highest lubricin promoter-driven luminescence, it also retained more lubricin within the construct vs. 14% GelMA/2% OMA. The 14% GelMA/2% OMA group had higher lubricin secretion and better shape stability over the 22 days in culture. Together these results support that the 14% GelMA/2% OMA after 15s crosslinking is an optimal combination for lubricin expression and 3D bioprinting of surface zone articular cartilage.

Overall Conclusion and Future Directions

This dissertation showed that combinations of biomaterials can stimulate specific ECM gene expression to recreate zonal articular cartilage, which was determined by using primary human

chondrocyte reporter cells. The results of this study have determined an optimal combination of GelMA:HAMA for type II collagen expression and GelMA/OMA for lubricin expression. This supports my overall hypothesis that zonal articular cartilage specific ECM gene expression can be stimulated by biomaterials, and they can be studied and optimized using primary human chondrocyte reporters.

With these final combinations the next step would be to determine the impact of increasing cell density. This would likely increase both type II collagen and lubricin expression. Once an optimal cell density has been determined for each section, then the surface zone will be 3D bioprinted on top of the deep zone. This dual layer construct can then be assessed for both lubricin and type II collagen expression. Then to engineer a full thickness osteochondral construct, the next step would be to determine the optimal biomaterials for the calcified cartilage section. However, the type II collagen expression in the GelMA:HAMA ratio could be improved upon. To pursue a balance between material degradation and ECM production, OMA could be added to this combination to slow the overall degradation rate. HAMA could also be added to the GelMA/OMA mixture to further improve the lubricin expression since lubricin has been shown to interact synergistically with hyaluronic acid [125]. To optimize the stiffness of the biomaterials or further determine the impact of stiffness on chondrogenesis, engineering reporter cells for aggrecan expression would be beneficial. Constructs could be bioprinted containing aggrecan promoter driven *Gaussia* luciferase and stiffness measured by DMA.

A difficulty with 3D bioprinting is the time it takes to print, even the simple disc constructs in this study. While we were able to maintain a high viability in the GelMA:HAMA combinations,

the viability with GelMA/OMA was slightly decreased. This could be attributed to the longer time taken to print a higher number of constructs. The time cells spend with the biomaterials is time spent without nutrients and limited oxygen. However, using temperature sensitive materials like GelMA requires time to reach an optimal bioprinting temperature. To simplify the 3D bioprinting process determining how long chondrocytes can reside within biomaterials before viability and chondrogenesis are negatively impacted would be beneficial. Alternatively, supplementing the PBS with glucose or some other cell nutrients when making the biomaterials could also improve viability during longer printing times.

APPENDIX A: SUPPLEMENTAL DATA FOR MIDDLE-DEEP ZONE RESULTS

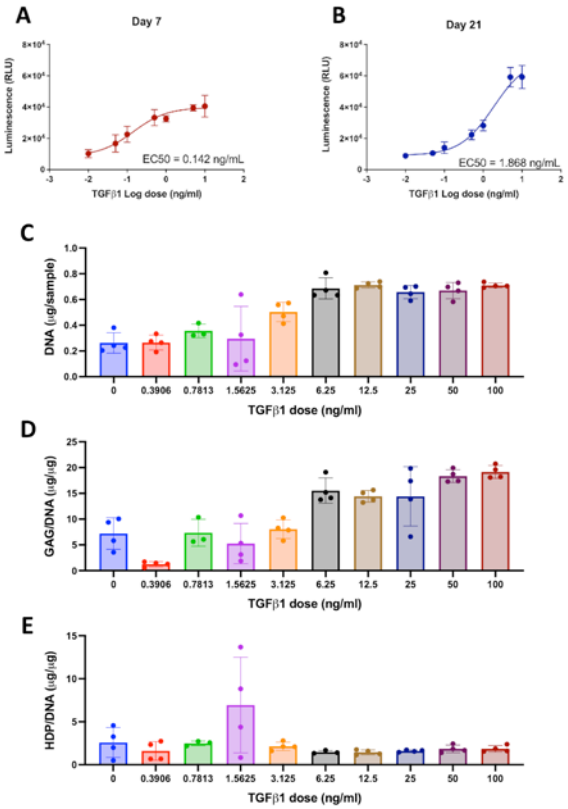

Figure 26S: HuCOL2gLuc reporter cells dose response to TGFβ1

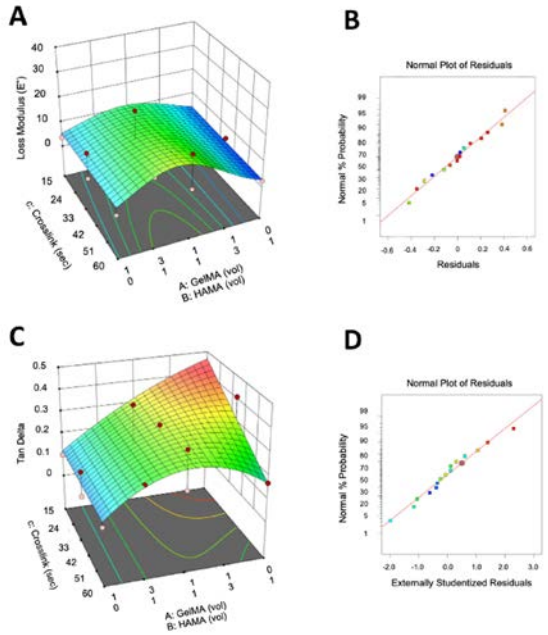

Figure 27S: 3D surface plots for loss moduli and tan delta for Day 0 and the corresponding normal probability plot of residuals

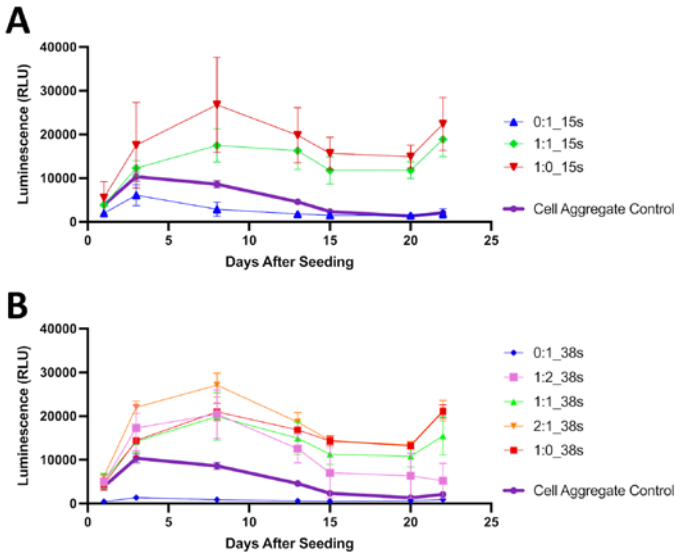

Figure 28S: GelMA:HAMA combinations after 15s or 38s crosslinking, including a cell aggregate control

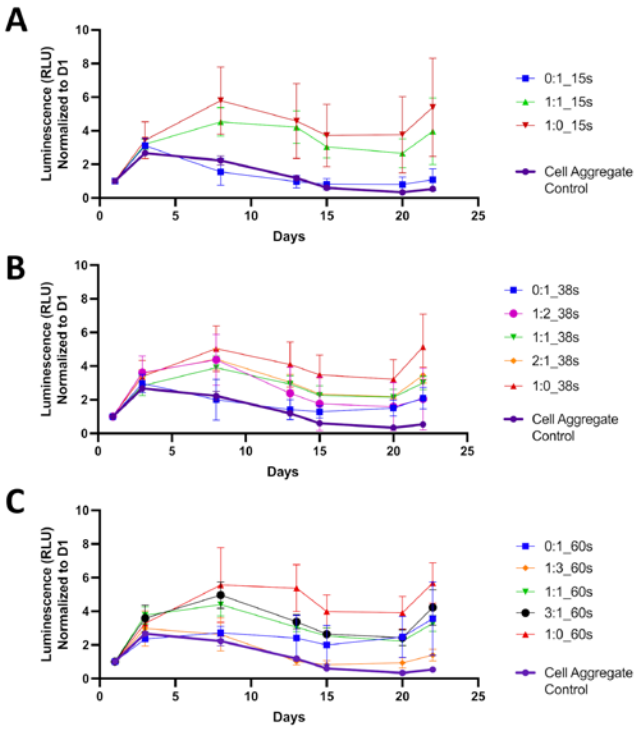

Figure 29S: GelMA:HAMA combinations with luminescence normalized to day 1 after 15s, 38s or 60s crosslinking, including a cell aggregate control

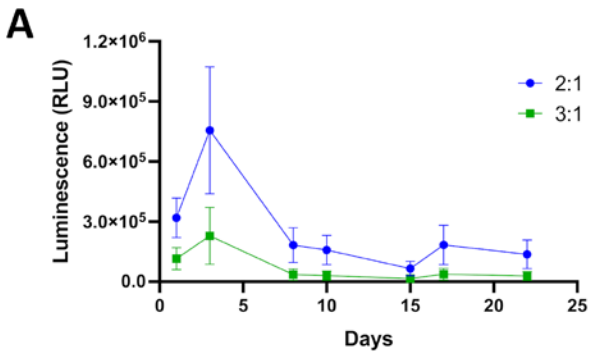

Figure 30S: Raw luminescence data for 3D bioprinted chondrocytes printed in GelMA:HAMA with ratios 2:1 and 3:1

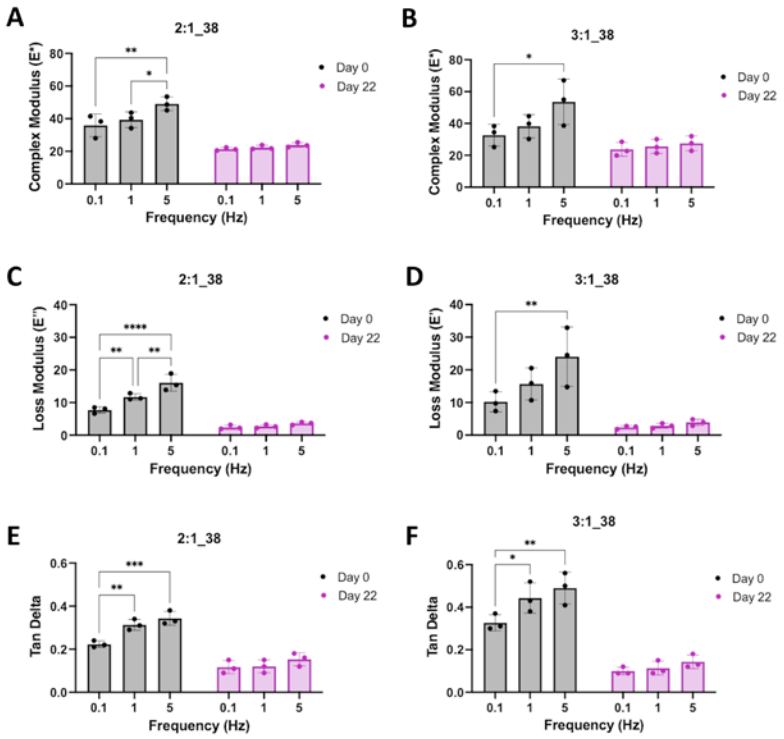

Figure 31S: Complex modulus, Loss modulus and Tan Delta for GelMA:HAMA 3D bioprints with ratios 2:1 and 3:1 on day 0 and day 22

APPENDIX B: SUPPLEMENTAL DATA FOR SURFACE ZONE RESULTS

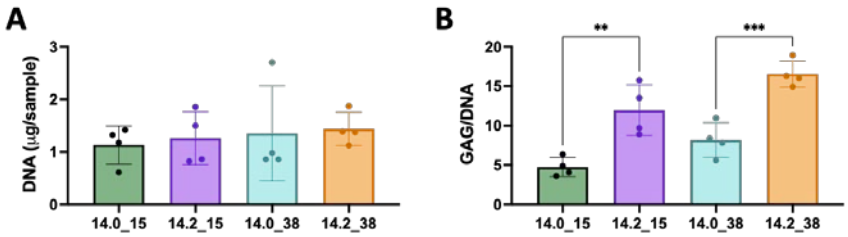

Figure 32S: DNA and GAG/DNA for 14% GelMA vs 14% GelMA/2% OMA from the validation

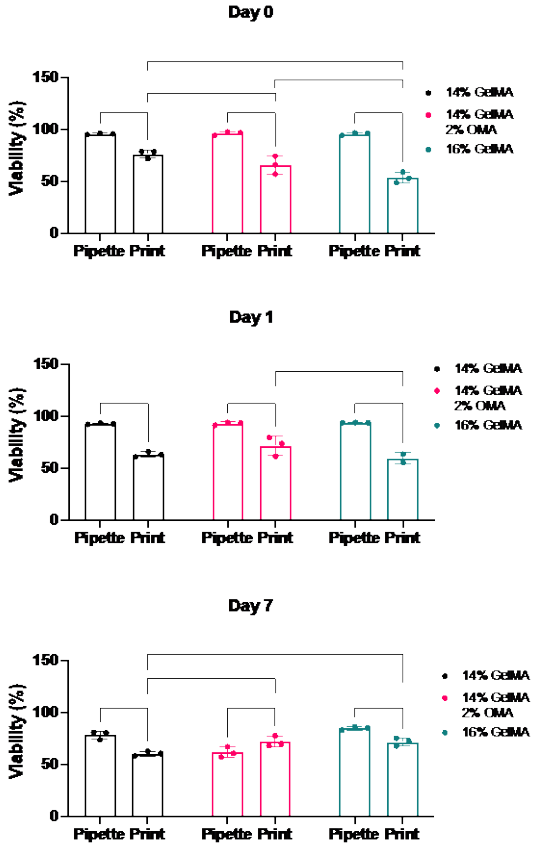

Figure 33S: Cell viability for 3D bioprinted groups vs pipetted controls on days 0, 1 and 7

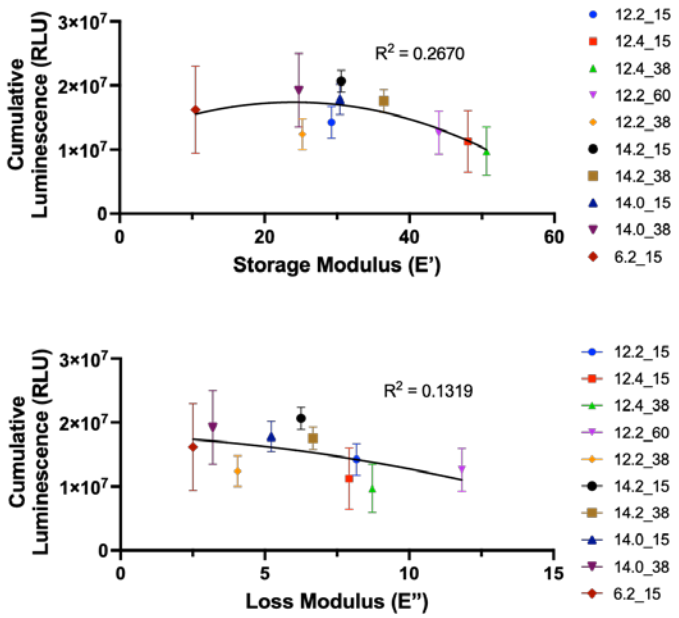

Figure 34S: Storage modulus and loss modulus vs cumulative luminescence

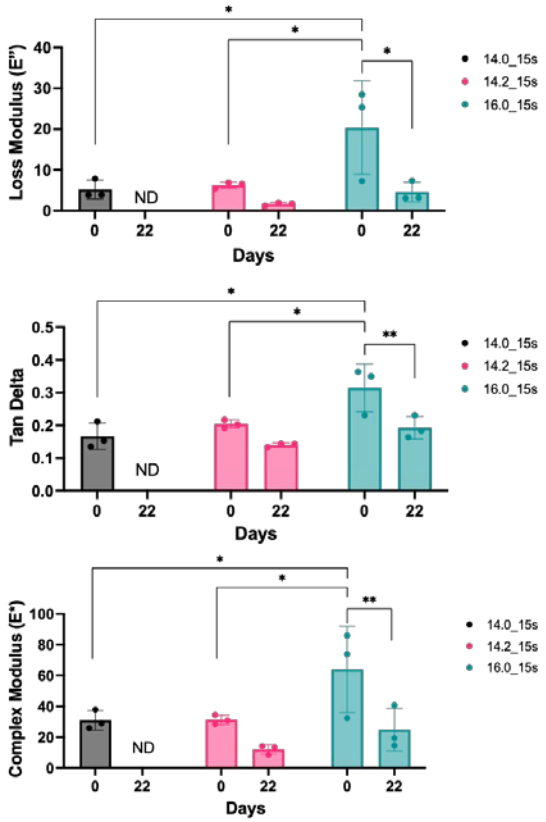

Figure 35S: Loss modulus, tan delta and cumulative modulus of 3D bioprinted constructs day 0 vs day 22

Table 4: Design of Experiment generated groups for surface zone optimization

Group	GelMA percent	OMA percent	Crosslinking time (s)	Calcium (yes/no)
1	0	2	15	Yes
2	0	2	15	No
3	0	2	38	Yes
4	0	2	38	No
5	0	2	60	Yes
6	1	1	15	Yes
7	1	1	15	No
8	1	1	38	Yes
9	1	1	60	Yes
10	1	1	60	No
11	2	0	15	Yes
12	2	0	15	No
13	2	0	38	Yes
14	2	0	38	Yes
15	2	0	38	No
16	2	0	60	Yes
17	6	2	15	Yes
18	6	2	15	No
19	6	2	38	Yes
20	6	2	38	No
21	6	2	60	Yes
22	6	2	60	No
23	6.5	1	38	Yes
24	6.5	1	38	Yes
25	6.5	1	38	Yes
26	6.5	1	38	No
27	6.5	1	38	No
28	6.5	1	38	No
29	6.5	1	38	Yes
30	6.5	1	38	Yes
31	6.5	1	38	Yes
32	6.5	1	38	No
33	6.5	1	38	No
34	6.5	1	38	No
35	6.5	1	15	Yes

36	6.5	1	15	Yes
37	6.5	1	15	No
38	6.5	1	15	No
39	6.5	1	60	Yes
40	6.5	1	60	Yes
41	7	0	15	Yes
42	7	0	15	No
43	7	0	38	Yes
44	7	0	60	No
45	9.25	1	60	No
46	12	2	15	Yes
47	12	2	15	No
48	12	2	38	Yes
49	12	2	38	No
50	12	2	60	No
51	12	2	60	Yes
52	12	0	15	Yes
53	12	0	15	No
54	12	0	38	Yes
55	12	0	38	No
56	12	0	60	Yes
57	12	1	60	Yes
58	12	1	15	Yes
59	12	1	15	No
60	12	1	38	Yes

LIST OF REFERENCES

[1] E.B. Hunziker, K. Lippuner, M.J.B. Keel, N. Shintani, An educational review of cartilage repair: precepts & practice – myths & misconceptions – progress & prospects, Osteoarthritis Cartilage. 23 (2015) 334–350. https://doi.org/10.1016/j.joca.2014.12.011.

[2] D. Drummer, J. McAdam, R. Seay, A. Ferrando, S.L. Bridges, J.A. Singh, M. Bamman, Osteoarthritis Progression: Mitigation and Rehabilitation Strategies, Front. Rehabil. Sci. 2 (2021). https://www.frontiersin.org/articles/10.3389/fresc.2021.724052 (accessed September 15, 2022).

[3] S. Glyn-Jones, A.J.R. Palmer, R. Agricola, A.J. Price, T.L. Vincent, H. Weinans, A.J. Carr, Osteoarthritis, The Lancet. 386 (2015) 376–387. https://doi.org/10.1016/S0140-6736(14)60802-3.

[4] A.E. Weber, I.K. Bolia, N.A. Trasolini, Biological strategies for osteoarthritis: from early diagnosis to treatment, Int. Orthop. 45 (2021) 335–344. https://doi.org/10.1007/s00264-020-04838-w.

[5] J.W. Bijlsma, F. Berenbaum, F.P. Lafeber, Osteoarthritis: an update with relevance for clinical practice, The Lancet. 377 (2011) 2115–2126. https://doi.org/10.1016/S0140-6736(11)60243-2.

[6] L. Punzi, P. Galozzi, R. Luisetto, M. Favero, R. Ramonda, F. Oliviero, A. Scanu, Post-traumatic arthritis: overview on pathogenic mechanisms and role of inflammation, RMD Open. 2 (2016) e000279. https://doi.org/10.1136/rmdopen-2016-000279.

[7] Y. Krishnan, A.J. Grodzinsky, Cartilage Diseases, Matrix Biol. J. Int. Soc. Matrix Biol. 71–72 (2018) 51–69. https://doi.org/10.1016/j.matbio.2018.05.005.

[8] A.J. Sophia Fox, A. Bedi, S.A. Rodeo, The Basic Science of Articular Cartilage, Sports Health. 1 (2009) 461–468. https://doi.org/10.1177/1941738109350438.

[9] T.I. Morales, Chondrocyte Moves: clever strategies?, Osteoarthr. Cartil. OARS Osteoarthr. Res. Soc. 15 (2007) 861–871. https://doi.org/10.1016/j.joca.2007.02.022.

[10] C. Hidaka, C. Cheng, D. Alexandre, M. Bhargava, P.A. Torzilli, Maturational differences in superficial and deep zone articular chondrocytes, Cell Tissue Res. 323 (2005) 127. https://doi.org/10.1007/s00441-005-0050-y.

[11] C. Chang, D.A. Lauffenburger, T.I. Morales, Motile chondrocytes from newborn calf: migration properties and synthesis of collagen II, Osteoarthritis Cartilage. 11 (2003) 603–612. https://doi.org/10.1016/S1063-4584(03)00087-6.

[12] T. Fujita, Y. Azuma, R. Fukuyama, Y. Hattori, C. Yoshida, M. Koida, K. Ogita, T. Komori, Runx2 induces osteoblast and chondrocyte differentiation and enhances their migration by coupling with PI3K-Akt signaling, J. Cell Biol. 166 (2004) 85–95. https://doi.org/10.1083/jcb.200401138.

[13] S.R. Frenkel, R.M. Clancy, J.L. Ricci, P.E. di Cesare, J.J. Rediske, S.B. Abramson, Effects of nitric oxide on chondrocyte migration, adhesion, and cytoskeletal assembly, Arthritis Rheum. 39 (1996) 1905–1912. https://doi.org/10.1002/art.1780391118.

[14] R. Mohan, N. Mohan, D. Vaikkath, Hyaluronic Acid Dictates Chondrocyte Morphology and Migration in Composite Gels, Tissue Eng. Part A. 24 (2018) 1481–1491. https://doi.org/10.1089/ten.tea.2017.0411.

[15] Y.-H. Tsai, C.-W. Chen, W.-F.T. Lai, J.-R. Tang, W.-P. Deng, S.-D. Yeh, A. Chung, C.S. Zuo, J.F. Bowley, Phenotypic changes in proliferation, differentiation, and migration of chondrocytes: 3D in vitro models for joint wound healing, J. Biomed. Mater. Res. A. 92A (2010) 1115–1122. https://doi.org/10.1002/jbm.a.32465.

[16] T.-K. Kim, B. Sharma, C.G. Williams, M.A. Ruffner, A. Malik, E.G. McFarland, J.H. Elisseeff, Experimental Model for Cartilage Tissue Engineering to Regenerate the Zonal Organization of Articular Cartilage, Osteoarthritis Cartilage. 11 (2003) 653–664. https://doi.org/10.1016/S1063-4584(03)00120-1.

[17] T.J. Klein, S.C. Rizzi, J.C. Reichert, N. Georgi, J. Malda, W. Schuurman, R.W. Crawford, D.W. Hutmacher, Strategies for Zonal Cartilage Repair using Hydrogels, Macromol. Biosci. 9 (2009) 1049–1058. https://doi.org/10.1002/mabi.200900176.

[18] N.G.M. Thielen, P.M. van der Kraan, A.P.M. van Caam, TGFβ/BMP Signaling Pathway in Cartilage Homeostasis, Cells. 8 (2019) 969. https://doi.org/10.3390/cells8090969.

[19] S. Kennedy, Using a Lubricin Reporter Cell to Test Current vs. Optimized Media Compositions, Honors Undergrad. Theses. (2021). https://stars.library.ucf.edu/honorstheses/891.

[20] D. Eyre, Articular cartilage and changes in Arthritis: Collagen of articular cartilage, Arthritis Res. 4 (2002) 30. https://doi.org/10.1186/ar380.

[21] G.A. Whitney, T.J. Kean, R.J. Fernandes, S. Waldman, M.Y. Tse, S.C. Pang, J.M. Mansour, J.E. Dennis, Thyroxine Increases Collagen Type II Expression and Accumulation in Scaffold-Free Tissue-Engineered Articular Cartilage, Tissue Eng. Part A. 24 (2018) 369–381. https://doi.org/10.1089/ten.tea.2016.0533.

[22] J.E. Dennis, T. Splawn, T.J. Kean, High-Throughput, Temporal and Dose Dependent, Effect of Vitamins and Minerals on Chondrogenesis, Front. Cell Dev. Biol. 8 (2020) 92. https://doi.org/10.3389/fcell.2020.00092.

[23] C.V. Gemmiti, R.E. Guldberg, Fluid Flow Increases Type II Collagen Deposition and Tensile Mechanical Properties in Bioreactor-Grown Tissue-Engineered Cartilage, Tissue Eng. 12 (2006) 469–479. https://doi.org/10.1089/ten.2006.12.469.

[24] K. Sato, H. Mera, S. Wakitani, M. Takagi, Effect of epigallocatechin-3-gallate on the increase in type II collagen accumulation in cartilage-like MSC sheets, Biosci. Biotechnol. Biochem. 81 (2017) 1241–1245. https://doi.org/10.1080/09168451.2017.1282809.

[25] H. Tian, B. Zhang, Q. Tian, Y. Liu, S. Yang, Z. Shao, Construction of self-assembled cartilage tissue from bone marrow mesenchymal stem cells induced by hypoxia combined with GDF-5, J. Huazhong Univ. Sci. Technolog. Med. Sci. 33 (2013) 700–706. https://doi.org/10.1007/s11596-013-1183-y.

[26] N. Mahmoudifar, P.M. Doran, Chondrogenic differentiation of human adipose-derived stem cells in polyglycolic acid mesh scaffolds under dynamic culture conditions, Biomaterials. 31 (2010) 3858–3867. https://doi.org/10.1016/j.biomaterials.2010.01.090.

[27] C. Kiani, L. Chen, Y.J. Wu, A.J. Yee, B.B. Yang, Structure and function of aggrecan, Cell Res. 12 (2002) 19–32. https://doi.org/10.1038/sj.cr.7290106.

[28] T. Niikura, A.H. Reddi, Differential regulation of lubricin/superficial zone protein by transforming growth factor β/bone morphogenetic protein superfamily members in

articular chondrocytes and synoviocytes, Arthritis Rheum. 56 (2007) 2312–2321. https://doi.org/10.1002/art.22659.

[29] Y. Lee, J. Choi, N.S. Hwang, Regulation of lubricin for functional cartilage tissue regeneration: a review, Biomater. Res. 22 (2018) 9. https://doi.org/10.1186/s40824-018-0118-x.

[30] D.P. Chang, N.I. Abu-Lail, J.M. Coles, F. Guilak, G.D. Jay, S. Zauscher, Friction force microscopy of lubricin and hyaluronic acid between hydrophobic and hydrophilic surfaces, Soft Matter. 5 (2009) 3438–3445. https://doi.org/10.1039/B907155E.

[31] D.K. Rhee, J. Marcelino, M. Baker, Y. Gong, P. Smits, V. Lefebvre, G.D. Jay, M. Stewart, H. Wang, M.L. Warman, J.D. Carpten, The secreted glycoprotein lubricin protects cartilage surfaces and inhibits synovial cell overgrowth, J. Clin. Invest. 115 (2005) 622–631. https://doi.org/10.1172/JCI22263.

[32] A.R. Watkins, H.L. Reesink, Lubricin in experimental and naturally occurring osteoarthritis: a systematic review, Osteoarthritis Cartilage. 28 (2020) 1303–1315. https://doi.org/10.1016/j.joca.2020.05.009.

[33] D. Nemirov, Y. Nakagawa, Z. Sun, A. Lebaschi, S. Wada, C. Carballo, X.-H. Deng, D. Putnam, L.J. Bonassar, S.A. Rodeo, Effect of Lubricin Mimetics on the Inhibition of Osteoarthritis in a Rat Anterior Cruciate Ligament Transection Model, Am. J. Sports Med. 48 (2020) 624–634. https://doi.org/10.1177/0363546519898691.

[34] C.R. Flannery, R. Zollner, C. Corcoran, A.R. Jones, A. Root, M.A. Rivera-Bermúdez, T. Blanchet, J.P. Gleghorn, L.J. Bonassar, A.M. Bendele, E.A. Morris, S.S. Glasson, Prevention of cartilage degeneration in a rat model of osteoarthritis by intraarticular

treatment with recombinant lubricin, Arthritis Rheum. 60 (2009) 840–847. https://doi.org/10.1002/art.24304.

[35] Z. Cui, C. Xu, X. Li, J. Song, B. Yu, Treatment with recombinant lubricin attenuates osteoarthritis by positive feedback loop between articular cartilage and subchondral bone in ovariectomized rats, Bone. 74 (2015) 37–47. https://doi.org/10.1016/j.bone.2014.12.065.

[36] A.P. Hollander, I. Pidoux, A. Reiner, C. Rorabeck, R. Bourne, A.R. Poole, Damage to type II collagen in aging and osteoarthritis starts at the articular surface, originates around chondrocytes, and extends into the cartilage with progressive degeneration., (1995). https://doi.org/10.1172/JCI118357.

[37] H.J. Häuselmann, J. Flechtenmacher, L. Michal, E.J.-M.A. Thonar, M. Shinmei, K.E. Kuettner, M.B. Aydelotte, The superficial layer of human articular cartilage is more susceptible to interleukin-1–induced damage than the deeper layers, Arthritis Rheum. 39 (1996) 478–488. https://doi.org/10.1002/art.1780390316.

[38] L. Fu, P. Li, H. Li, C. Gao, Z. Yang, T. Zhao, W. Chen, Z. Liao, Y. Peng, F. Cao, X. Sui, S. Liu, Q. Guo, The Application of Bioreactors for Cartilage Tissue Engineering: Advances, Limitations, and Future Perspectives, Stem Cells Int. 2021 (2021) e6621806. https://doi.org/10.1155/2021/6621806.

[39] S. Caddeo, M. Boffito, S. Sartori, Tissue Engineering Approaches in the Design of Healthy and Pathological In Vitro Tissue Models, Front. Bioeng. Biotechnol. 5 (2017). https://www.frontiersin.org/article/10.3389/fbioe.2017.00040 (accessed March 10, 2022).

[40] F. You, B.F. Eames, X. Chen, Application of Extrusion-Based Hydrogel Bioprinting for Cartilage Tissue Engineering, Int. J. Mol. Sci. 18 (2017) 1597. https://doi.org/10.3390/ijms18071597.

[41] L. Zhang, G. Yang, B.N. Johnson, X. Jia, Three-dimensional (3D) printed scaffold and material selection for bone repair, Acta Biomater. 84 (2019) 16–33. https://doi.org/10.1016/j.actbio.2018.11.039.

[42] T.J. Kean, M. Thanou, Utility of Chitosan for 3D Printing and Bioprinting, in: G. Crini, E. Lichtfouse (Eds.), Sustain. Agric. Rev. 35 Chitin Chitosan Hist. Fundam. Innov., Springer International Publishing, Cham, 2019: pp. 271–292. https://doi.org/10.1007/978-3-030-16538-3_6.

[43] R.L. Pan, K. Martyniak, M. Karimzadeh, D.G. Gelikman, J. DeVries, K. Sutter, M. Coathup, M. Razavi, R. Sawh-Martinez, T.J. Kean, Systematic review on the application of 3D-bioprinting technology in orthoregeneration: current achievements and open challenges, J. Exp. Orthop. 9 (2022) 95. https://doi.org/10.1186/s40634-022-00518-3.

[44] A.C. Daly, D.J. Kelly, Biofabrication of spatially organised tissues by directing the growth of cellular spheroids within 3D printed polymeric microchambers, Biomaterials. 197 (2019) 194–206. https://doi.org/10.1016/j.biomaterials.2018.12.028.

[45] B.P. Chan, K.W. Leong, Scaffolding in tissue engineering: general approaches and tissue-specific considerations, Eur. Spine J. 17 (2008) 467–479. https://doi.org/10.1007/s00586-008-0745-3.

[46] A.C. Daly, M.E. Prendergast, A.J. Hughes, J.A. Burdick, Bioprinting for the Biologist, Cell. 184 (2021) 18–32. https://doi.org/10.1016/j.cell.2020.12.002.

[47] A. Leucht, A.-C. Volz, J. Rogal, K. Borchers, P.J. Kluger, Advanced gelatin-based vascularization bioinks for extrusion-based bioprinting of vascularized bone equivalents, Sci. Rep. 10 (2020) 5330. https://doi.org/10.1038/s41598-020-62166-w.

[48] M. Zhu, Y. Wang, G. Ferracci, J. Zheng, N.-J. Cho, B.H. Lee, Gelatin methacryloyl and its hydrogels with an exceptional degree of controllability and batch-to-batch consistency, Sci. Rep. 9 (2019) 6863. https://doi.org/10.1038/s41598-019-42186-x.

[49] A.C. Daly, S.E. Critchley, E.M. Rencsok, D.J. Kelly, A comparison of different bioinks for 3D bioprinting of fibrocartilage and hyaline cartilage, Biofabrication. 8 (2016) 045002. https://doi.org/10.1088/1758-5090/8/4/045002.

[50] K. Yue, G.T. Santiago, M.M. Alvarez, A. Tamayol, N. Annabi, A. Khademhosseini, Synthesis, properties, and biomedical applications of gelatin methacryloyl (GelMA) hydrogels, Biomaterials. 73 (2015) 254–271. https://doi.org/10.1016/j.biomaterials.2015.08.045.

[51] S. Bertlein, G. Brown, K.S. Lim, T. Jungst, T. Boeck, T. Blunk, J. Tessmar, G.J. Hooper, T.B.F. Woodfield, J. Groll, Thiol–Ene Clickable Gelatin: A Platform Bioink for Multiple 3D Biofabrication Technologies, Adv. Mater. 29 (2017) 1703404. https://doi.org/10.1002/adma.201703404.

[52] A.I. Van Den Bulcke, B. Bogdanov, N. De Rooze, E.H. Schacht, M. Cornelissen, H. Berghmans, Structural and Rheological Properties of Methacrylamide Modified Gelatin Hydrogels, Biomacromolecules. 1 (2000) 31–38. https://doi.org/10.1021/bm990017d.

[53] S. Bupphathong, C. Quiroz, W. Huang, P.-F. Chung, H.-Y. Tao, C.-H. Lin, Gelatin Methacrylate Hydrogel for Tissue Engineering Applications—A Review on Material Modifications, Pharmaceuticals. 15 (2022) 171. https://doi.org/10.3390/ph15020171.

[54] C.L. Nemeth, K. Janebodin, A.E. Yuan, J.E. Dennis, M. Reyes, D.-H. Kim, Enhanced Chondrogenic Differentiation of Dental Pulp Stem Cells Using Nanopatterned PEG-GelMA-HA Hydrogels, Tissue Eng. Part A. 20 (2014) 2817–2829. https://doi.org/10.1089/ten.tea.2013.0614.

[55] M. Guvendiren, J.A. Burdick, Stiffening hydrogels to probe short- and long-term cellular responses to dynamic mechanics, Nat. Commun. 3 (2012) 792. https://doi.org/10.1038/ncomms1792.

[56] G. Camci-Unal, J.W. Nichol, H. Bae, H. Tekin, J. Bischoff, A. Khademhosseini, Hydrogel Surfaces to Promote Attachment and Spreading of Endothelial Progenitor Cells, J. Tissue Eng. Regen. Med. 7 (2013) 337–347. https://doi.org/10.1002/term.517.

[57] G. Camci-Unal, D. Cuttica, N. Annabi, D. Demarchi, A. Khademhosseini, Synthesis and Characterization of Hybrid Hyaluronic Acid-Gelatin Hydrogels, Biomacromolecules. 14 (2013) 1085–1092. https://doi.org/10.1021/bm3019856.

[58] S. Nedunchezian, P. Banerjee, C.-Y. Lee, S.-S. Lee, C.-W. Lin, C.-W. Wu, S.-C. Wu, J.-K. Chang, C.-K. Wang, Generating adipose stem cell-laden hyaluronic acid-based scaffolds using 3D bioprinting via the double crosslinked strategy for chondrogenesis, Mater. Sci. Eng. C. 124 (2021) 112072. https://doi.org/10.1016/j.msec.2021.112072.

[59] O. Jeon, K.H. Bouhadir, J.M. Mansour, E. Alsberg, Photocrosslinked alginate hydrogels with tunable biodegradation rates and mechanical properties, Biomaterials. 30 (2009) 2724–2734. https://doi.org/10.1016/j.biomaterials.2009.01.034.

[60] O. Jeon, D.S. Alt, S.M. Ahmed, E. Alsberg, The effect of oxidation on the degradation of photocrosslinkable alginate hydrogels, Biomaterials. 33 (2012) 3503–3514. https://doi.org/10.1016/j.biomaterials.2012.01.041.

[61] O. Jeon, Y.B. Lee, S.J. Lee, N. Guliyeva, J. Lee, E. Alsberg, Stem cell-laden hydrogel bioink for generation of high resolution and fidelity engineered tissues with complex geometries, Bioact. Mater. 15 (2022) 185–193. https://doi.org/10.1016/j.bioactmat.2021.11.025.

[62] O. Jeon, Y.B. Lee, H. Jeong, S.J. Lee, D. Wells, E. Alsberg, Individual cell-only bioink and photocurable supporting medium for 3D printing and generation of engineered tissues with complex geometries, Mater. Horiz. 6 (2019) 1625–1631. https://doi.org/10.1039/C9MH00375D.

[63] B.D. Fairbanks, M.P. Schwartz, C.N. Bowman, K.S. Anseth, Photoinitiated polymerization of PEG-diacrylate with lithium phenyl-2,4,6-trimethylbenzoylphosphinate: polymerization rate and cytocompatibility, Biomaterials. 30 (2009) 6702–6707. https://doi.org/10.1016/j.biomaterials.2009.08.055.

[64] H. Xu, J. Casillas, S. Krishnamoorthy, C. Xu, Effects of Irgacure 2959 and lithium phenyl-2,4,6-trimethylbenzoylphosphinate on cell viability, physical properties, and microstructure in 3D bioprinting of vascular-like constructs, Biomed. Mater. 15 (2020) 055021. https://doi.org/10.1088/1748-605X/ab954e.

[65] A.K. Nguyen, P.L. Goering, V. Reipa, R.J. Narayan, Toxicity and photosensitizing assessment of gelatin methacryloyl-based hydrogels photoinitiated with lithium phenyl-2,4,6-trimethylbenzoylphosphinate in human primary renal proximal tubule epithelial cells, Biointerphases. 14 (2019) 021007. https://doi.org/10.1116/1.5095886.

[66] K. Martyniak, A. Lokshina, M.A. Cruz, M. Karimzadeh, R. Kemp, T.J. Kean, Biomaterial composition and stiffness as decisive properties of 3D bioprinted constructs for type II collagen stimulation, Acta Biomater. (2022). https://doi.org/10.1016/j.actbio.2022.08.058.

[67] O. Ly, F. Monchau, S. Rémond, C. Lors, A. Jouanneaux, É. Debarre, D. Damidot, Optimization of the formulation of an original hydrogel-based bone cement using a mixture design, J. Mech. Behav. Biomed. Mater. 110 (2020) 103886. https://doi.org/10.1016/j.jmbbm.2020.103886.

[68] L. Eriksson, E. Johansson, C. Wikström, Mixture design—design generation, PLS analysis, and model usage, Chemom. Intell. Lab. Syst. 43 (1998) 1–24. https://doi.org/10.1016/S0169-7439(98)00126-9.

[69] J. Lam, S.T. Carmichael, W.E. Lowry, T. Segura, Design of experiments methodology to optimize hydrogel for iPSC-NPC culture, Adv. Healthc. Mater. 4 (2015) 534–539. https://doi.org/10.1002/adhm.201400410.

[70] J.L. Cook, A.M. Stoker, J.P. Stannard, K. Kuroki, C.R. Cook, F.M. Pfeiffer, C. Bozynski, C.T. Hung, A Novel System Improves Preservation of Osteochondral Allografts, Clin. Orthop. 472 (2014) 3404–3414. https://doi.org/10.1007/s11999-014-3773-9.

[71] D.P. Lennon, S.E. Haynesworth, S.P. Bruder, N. Jaiswal, A.I. Caplan, Human and Animal Mesenchymal Progenitor Cells from Bone Marrow: Identification of Serum for Optimal Selection and Proliferation, In Vitro Cell. Dev. Biol. Anim. 32 (1996) 602–611.

[72] T.J. Kean, J.E. Dennis, Synoviocyte Derived-Extracellular Matrix Enhances Human Articular Chondrocyte Proliferation and Maintains Re-Differentiation Capacity at

Both Low and Atmospheric Oxygen Tensions, PLOS ONE. 10 (2015) e0129961. https://doi.org/10.1371/journal.pone.0129961.

[73] R. Truong, M. Bernier, J.E. Dennis, T.J. Kean, Synoviocyte-derived extracellular matrix and bFGF speed human chondrocyte proliferation while maintaining differentiation potential, Front. Bioeng. Biotechnol. (2022). https://www.frontiersin.org/articles/10.3389/fbioe.2022.825005/abstract.

[74] U. Schmidt, M. Weigert, C. Broaddus, G. Myers, Cell Detection with Star-convex Polygons, ArXiv180603535 Cs. 11071 (2018) 265–273. https://doi.org/10.1007/978-3-030-00934-2_30.

[75] J.E. Dennis, G.A. Whitney, J. Rai, R.J. Fernandes, T.J. Kean, Physioxia Stimulates Extracellular Matrix Deposition and Increases Mechanical Properties of Human Chondrocyte-Derived Tissue-Engineered Cartilage, Front. Bioeng. Biotechnol. 8 (2020). https://www.frontiersin.org/article/10.3389/fbioe.2020.590743 (accessed March 18, 2022).

[76] T.J. Kean, H. Mera, G.A. Whitney, D.L. MacKay, A. Awadallah, R.J. Fernandes, J.E. Dennis, Disparate response of articular- and auricular-derived chondrocytes to oxygen tension, Connect. Tissue Res. 57 (2016) 319–333. https://doi.org/10.1080/03008207.2016.1182996.

[77] C. Zheng, M.E. Levenston, Fact versus artifact: Avoiding erroneous estimates of sulfated glycosaminoglycan content using the dimethylmethylene blue colorimetric assay for tissue-engineered constructs, Eur. Cell. Mater. 29 (2015) 224–236.

[78] H.A. Pedrozo, Z. Schwartz, R. Gomez, A. Ornoy, W. Xin-Sheng, S.L. Dallas, L.F. Bonewald, D.D. Dean, B.D. Boyan, Growth plate chondrocytes store latent

transforming growth factor (TGF)-β1 in their matrix through latent TGF-β1 binding protein-1, J. Cell. Physiol. 177 (1998) 343–354. https://doi.org/10.1002/(SICI)1097-4652(199811)177:2<343::AID-JCP16>3.0.CO;2-A.

[79] J.T. March, G. Golshirazi, V. Cernisova, H. Carr, Y. Leong, N. Lu-Nguyen, L.J. Popplewell, Targeting TGFβ Signaling to Address Fibrosis Using Antisense Oligonucleotides, Biomedicines. 6 (2018) 74. https://doi.org/10.3390/biomedicines6030074.

[80] P. Galéra, D. Vivien, S. Pronost, J. Bonaventure, F. Rédini, G. Loyau, J.-P. Pujol, Transforming growth factor-β1 (TGF-β1) up-regulation of collagen type II in primary cultures of rabbit articular chondrocytes (RAC) involves increased mRNA levels without affecting mRNA stability and procollagen processing, J. Cell. Physiol. 153 (1992) 596–606. https://doi.org/10.1002/jcp.1041530322.

[81] R.A. Ignotz, J. Massagué, Transforming growth factor-beta stimulates the expression of fibronectin and collagen and their incorporation into the extracellular matrix., J. Biol. Chem. 261 (1986) 4337–4345. https://doi.org/10.1016/S0021-9258(17)35666-1.

[82] T.A. Schmidt, N.S. Gastelum, E.H. Han, G.E. Nugent-Derfus, B.L. Schumacher, R.L. Sah, Differential regulation of proteoglycan 4 metabolism in cartilage by IL-1α, IGF-I, and TGF-β1, Osteoarthritis Cartilage. 16 (2008) 90–97. https://doi.org/10.1016/j.joca.2007.05.009.

[83] S. Giovannini, J. Diaz-Romero, T. Aigner, P. Mainil-Varlet, D. Nesic, Population doublings and percentage of S100-positive cells as predictors of in vitro chondrogenicity of expanded human articular chondrocytes, J. Cell. Physiol. 222 (2010) 411–420. https://doi.org/10.1002/jcp.21965.

[84] B. Kessel, M. Lee, A. Bonato, Y. Tinguely, E. Tosoratti, M. Zenobi-Wong, 3D Bioprinting of Macroporous Materials Based on Entangled Hydrogel Microstrands, Adv. Sci. 7 (2020) 2001419. https://doi.org/10.1002/advs.202001419.

[85] T. Lam, T. Dehne, J.P. Krüger, S. Hondke, M. Endres, A. Thomas, R. Lauster, M. Sittinger, L. Kloke, Photopolymerizable gelatin and hyaluronic acid for stereolithographic 3D bioprinting of tissue-engineered cartilage, J. Biomed. Mater. Res. B Appl. Biomater. 107 (2019) 2649–2657. https://doi.org/10.1002/jbm.b.34354.

[86] C.D. O'Connell, C. Onofrillo, S. Duchi, X. Li, Y. Zhang, P. Tian, L. Lu, A. Trengove, A. Quigley, S. Gambhir, A. Khansari, T. Mladenovska, A. O'Connor, C.D. Bella, P.F. Choong, G.G. Wallace, Evaluation of sterilisation methods for bio-ink components: gelatin, gelatin methacryloyl, hyaluronic acid and hyaluronic acid methacryloyl, Biofabrication. 11 (2019) 035003. https://doi.org/10.1088/1758-5090/ab0b7c.

[87] M. Costantini, J. Idaszek, K. Szöke, J. Jaroszewicz, M. Dentini, A. Barbetta, J.E. Brinchmann, W. Święszkowski, 3D bioprinting of BM-MSCs-loaded ECM biomimetic hydrogels for in vitro neocartilage formation, Biofabrication. 8 (2016) 035002. https://doi.org/10.1088/1758-5090/8/3/035002.

[88] Y. Fan, Z. Yue, E. Lucarelli, G.G. Wallace, Hybrid Printing Using Cellulose Nanocrystals Reinforced GelMA/HAMA Hydrogels for Improved Structural Integration, Adv. Healthc. Mater. 9 (2020) 2001410. https://doi.org/10.1002/adhm.202001410.

[89] V.H.M. Mouser, R. Levato, A. Mensinga, W.J.A. Dhert, D. Gawlitta, J. Malda, Bio-ink development for three-dimensional bioprinting of hetero-cellular cartilage constructs, Connect. Tissue Res. 61 (2020) 137–151. https://doi.org/10.1080/03008207.2018.1553960.

[90] J. Idaszek, M. Costantini, T.A. Karlsen, J. Jaroszewicz, C. Colosi, S. Testa, E. Fornetti, S. Bernardini, M. Seta, K. Kasare\l\lo, R. Wrzesień, S. Cannata, A. Barbetta, C. Gargioli, J.E. Brinchman, W. Święszkowski, 3D bioprinting of hydrogel constructs with cell and material gradients for the regeneration of full-thickness chondral defect using a microfluidic printing head, Biofabrication. 11 (2019) 044101. https://doi.org/10.1088/1758-5090/ab2622.

[91] C. Onofrillo, S. Duchi, C.D. O'Connell, R. Blanchard, A.J. O'Connor, M. Scott, G.G. Wallace, P.F.M. Choong, C.D. Bella, Biofabrication of human articular cartilage: a path towards the development of a clinical treatment, Biofabrication. 10 (2018) 045006. https://doi.org/10.1088/1758-5090/aad8d9.

[92] C. Di Bella, S. Duchi, C.D. O'Connell, R. Blanchard, C. Augustine, Z. Yue, F. Thompson, C. Richards, S. Beirne, C. Onofrillo, S.H. Bauquier, S.D. Ryan, P. Pivonka, G.G. Wallace, P.F. Choong, In situ handheld three-dimensional bioprinting for cartilage regeneration, J. Tissue Eng. Regen. Med. 12 (2018) 611–621. https://doi.org/10.1002/term.2476.

[93] C.D. O'Connell, C.D. Bella, F. Thompson, C. Augustine, S. Beirne, R. Cornock, C.J. Richards, J. Chung, S. Gambhir, Z. Yue, J. Bourke, B. Zhang, A. Taylor, A. Quigley, R. Kapsa, P. Choong, G.G. Wallace, Development of the Biopen: a handheld device for surgical printing of adipose stem cells at a chondral wound site, Biofabrication. 8 (2016) 015019. https://doi.org/10.1088/1758-5090/8/1/015019.

[94] J. Hauptstein, T. Böck, M. Bartolf-Kopp, L. Forster, P. Stahlhut, A. Nadernezhad, G. Blahetek, A. Zernecke-Madsen, R. Detsch, T. Jüngst, J. Groll, J. Teßmar, T. Blunk, Hyaluronic Acid-Based Bioink Composition Enabling 3D Bioprinting and Improving

Quality of Deposited Cartilaginous Extracellular Matrix, Adv. Healthc. Mater. 9 (2020) 2000737. https://doi.org/10.1002/adhm.202000737.

[95] R. Schipani, S. Scheurer, R. Florentin, S.E. Critchley, D.J. Kelly, Reinforcing interpenetrating network hydrogels with 3D printed polymer networks to engineer cartilage mimetic composites, Biofabrication. 12 (2020) 035011. https://doi.org/10.1088/1758-5090/ab8708.

[96] L. Ruiz-Cantu, A. Gleadall, C. Faris, J. Segal, K. Shakesheff, J. Yang, Multi-material 3D bioprinting of porous constructs for cartilage regeneration, Mater. Sci. Eng. C. 109 (2020) 110578. https://doi.org/10.1016/j.msec.2019.110578.

[97] T. Wang, J.H. Lai, F. Yang, Effects of Hydrogel Stiffness and Extracellular Compositions on Modulating Cartilage Regeneration by Mixed Populations of Stem Cells and Chondrocytes In Vivo, Tissue Eng. Part A. 22 (2016) 1348–1356. https://doi.org/10.1089/ten.tea.2016.0306.

[98] B. Bachmann, S. Spitz, B. Schädl, A.H. Teuschl, H. Redl, S. Nürnberger, P. Ertl, Stiffness Matters: Fine-Tuned Hydrogel Elasticity Alters Chondrogenic Redifferentiation, Front. Bioeng. Biotechnol. 8 (2020). https://www.frontiersin.org/article/10.3389/fbioe.2020.00373 (accessed May 25, 2022).

[99] J.M. Patel, B.C. Wise, E.D. Bonnevie, R.L. Mauck, A Systematic Review and Guide to Mechanical Testing for Articular Cartilage Tissue Engineering, Tissue Eng. Part C Methods. 25 (2019) 593–608. https://doi.org/10.1089/ten.tec.2019.0116.

[100] A. Fallacara, E. Baldini, S. Manfredini, S. Vertuani, Hyaluronic Acid in the Third Millennium, Polymers. 10 (2018) 701. https://doi.org/10.3390/polym10070701.

[101] O. Ishida, Y. Tanaka, I. Morimoto, M. Takigawa, S. Eto, Chondrocytes Are Regulated by Cellular Adhesion Through CD44 and Hyaluronic Acid Pathway, J. Bone Miner. Res. 12 (1997) 1657–1663. https://doi.org/10.1359/jbmr.1997.12.10.1657.

[102] E.A. Turley, P.W. Noble, L.Y.W. Bourguignon, Signaling Properties of Hyaluronan Receptors*, J. Biol. Chem. 277 (2002) 4589–4592. https://doi.org/10.1074/jbc.R100038200.

[103] A.J. Freemont, V. Hampson, R. Tilman, P. Goupille, Y. Taiwo, J.A. Hoyland, Gene expression of matrix metalloproteinases 1, 3, and 9 by chondrocytes in osteoarthritic human knee articular cartilage is zone and grade specific, Ann. Rheum. Dis. 56 (1997) 542–548. https://doi.org/10.1136/ard.56.9.542.

[104] A.P. Newman, Articular Cartilage Repair, Am. J. Sports Med. 26 (1998) 309–324. https://doi.org/10.1177/03635465980260022701.

[105] J.L. Cook, J.P. Stannard, A.M. Stoker, C.C. Bozynski, K. Kuroki, C.R. Cook, F.M. Pfeiffer, Importance of Donor Chondrocyte Viability for Osteochondral Allografts, Am. J. Sports Med. 44 (2016) 1260–1268. https://doi.org/10.1177/0363546516629434.

[106] O. Chaudhuri, L. Gu, M. Darnell, D. Klumpers, S.A. Bencherif, J.C. Weaver, N. Huebsch, D.J. Mooney, Substrate stress relaxation regulates cell spreading, Nat. Commun. 6 (2015) 6365. https://doi.org/10.1038/ncomms7365.

[107] C. Antich, J. de Vicente, G. Jiménez, C. Chocarro, E. Carrillo, E. Montañez, P. Gálvez-Martín, J.A. Marchal, Bio-inspired hydrogel composed of hyaluronic acid and alginate as a potential bioink for 3D bioprinting of articular cartilage engineering

constructs, Acta Biomater. 106 (2020) 114–123. https://doi.org/10.1016/j.actbio.2020.01.046.

[108] A. Kosik-Kozio\l, M. Costantini, T. Bolek, K. Szöke, A. Barbetta, J. Brinchmann, W. Święszkowski, PLA short sub-micron fiber reinforcement of 3D bioprinted alginate constructs for cartilage regeneration, Biofabrication. 9 (2017) 044105. https://doi.org/10.1088/1758-5090/aa90d7.

[109] X. Cui, K. Breitenkamp, M.G. Finn, M. Lotz, D.D. D'Lima, Direct Human Cartilage Repair Using Three-Dimensional Bioprinting Technology, Tissue Eng. Part A. 18 (2012) 1304–1312. https://doi.org/10.1089/ten.tea.2011.0543.

[110] J.M. Mansour, Biomechanics of Cartilage in Kinesiology: The Mechanics and Pathomechanics of Human Movement, Lippincot Williams & Wilkins, 2009. https://web.mit.edu/cortiz/www/3.052/3.052CourseReader/27_BiomechanicsofCartilage.pdf.

[111] B. Wang, P.J. Díaz-Payno, D.C. Browe, F.E. Freeman, J. Nulty, R. Burdis, D.J. Kelly, Affinity-bound growth factor within sulfated interpenetrating network bioinks for bioprinting cartilaginous tissues, Acta Biomater. 128 (2021) 130–142. https://doi.org/10.1016/j.actbio.2021.04.016.

[112] R. Levato, W.R. Webb, I.A. Otto, A. Mensinga, Y. Zhang, M. van Rijen, R. van Weeren, I.M. Khan, J. Malda, The bio in the ink: cartilage regeneration with bioprintable hydrogels and articular cartilage-derived progenitor cells, Acta Biomater. 61 (2017) 41–53. https://doi.org/10.1016/j.actbio.2017.08.005.

[113] A.C. Daly, G.M. Cunniffe, B.N. Sathy, O. Jeon, E. Alsberg, D.J. Kelly, 3D Bioprinting of Developmentally Inspired Templates for Whole Bone Organ

Engineering, Adv. Healthc. Mater. 5 (2016) 2353–2362. https://doi.org/10.1002/adhm.201600182.

[114] A. Kosik-Kozio\l, M. Costantini, A. Mróz, J. Idaszek, M. Heljak, J. Jaroszewicz, E. Kijeńska, K. Szöke, N. Frerker, A. Barbetta, J.E. Brinchmann, W. Święszkowski, 3D bioprinted hydrogel model incorporating $\upbeta$ -tricalcium phosphate for calcified cartilage tissue engineering, Biofabrication. 11 (2019) 035016. https://doi.org/10.1088/1758-5090/ab15cb.

[115] K.S. Lim, R. Levato, P.F. Costa, M.D. Castilho, C.R. Alcala-Orozco, K.M.A. van Dorenmalen, F.P.W. Melchels, D. Gawlitta, G.J. Hooper, J. Malda, T.B.F. Woodfield, Bio-resin for high resolution lithography-based biofabrication of complex cell-laden constructs, Biofabrication. 10 (2018) 034101. https://doi.org/10.1088/1758-5090/aac00c.

[116] G. Irmak, M. Gümüşderelioğlu, Photo-activated platelet-rich plasma (PRP)-based patient-specific bio-ink for cartilage tissue engineering, Biomed. Mater. 15 (2020) 065010. https://doi.org/10.1088/1748-605X/ab9e46.

[117] L. De Moor, S. Fernandez, C. Vercruysse, L. Tytgat, M. Asadian, N. De Geyter, S. Van Vlierberghe, P. Dubruel, H. Declercq, Hybrid Bioprinting of Chondrogenically Induced Human Mesenchymal Stem Cell Spheroids, Front. Bioeng. Biotechnol. 8 (2020) 484. https://doi.org/10.3389/fbioe.2020.00484.

[118] Y. Gu, L. Zhang, X. Du, Z. Fan, L. Wang, W. Sun, Y. Cheng, Y. Zhu, C. Chen, Reversible physical crosslinking strategy with optimal temperature for 3D bioprinting of human chondrocyte-laden gelatin methacryloyl bioink, J. Biomater. Appl. 33 (2018) 609–618. https://doi.org/10.1177/0885328218805864.

[119] W. Zhu, H. Cui, B. Boualam, F. Masood, E. Flynn, R.D. Rao, Z.-Y. Zhang, L.G. Zhang, 3D bioprinting mesenchymal stem cell-laden construct with core–shell nanospheres for cartilage tissue engineering, Nanotechnology. 29 (2018) 185101. https://doi.org/10.1088/1361-6528/aaafa1.

[120] C. Luo, R. Xie, J. Zhang, Y. Liu, Z. Li, Y. Zhang, X. Zhang, T. Yuan, Y. Chen, W. Fan, Low-Temperature Three-Dimensional Printing of Tissue Cartilage Engineered with Gelatin Methacrylamide, Tissue Eng. Part C Methods. 26 (2020) 306–316. https://doi.org/10.1089/ten.tec.2020.0053.

[121] K.Y. Lee, D.J. Mooney, Alginate: properties and biomedical applications, Prog. Polym. Sci. 37 (2012) 106–126. https://doi.org/10.1016/j.progpolymsci.2011.06.003.

[122] K. Martyniak, A. Lokshina, M.A. Cruz, M. Karimzadeh, R. Kemp, T.J. Kean, Biomaterial composition and stiffness as decisive properties of 3D bioprinted constructs for type II collagen stimulation, Acta Biomater. (2022). https://doi.org/10.1016/j.actbio.2022.08.058.

[123] D.P. Chang, F. Guilak, G. Jay, S. Zauscher, Interaction of Lubricin with Collagen II Surfaces: Adsorption, Friction, and Normal Forces, J. Biomech. 47 (2014) 659–666. https://doi.org/10.1016/j.jbiomech.2013.11.048.

[124] K.D. Jadin, B.L. Wong, W.C. Bae, K.W. Li, A.K. Williamson, B.L. Schumacher, J.H. Price, R.L. Sah, Depth-varying Density and Organization of Chondrocytes in Immature and Mature Bovine Articular Cartilage Assessed by 3D Imaging and Analysis, J. Histochem. Cytochem. 53 (2005) 1109–1119. https://doi.org/10.1369/jhc.4A6511.2005.

[125] H. Ye, M. Han, R. Huang, T.A. Schmidt, W. Qi, Z. He, L.L. Martin, G.D. Jay, R. Su, G.W. Greene, Interactions between Lubricin and Hyaluronic Acid Synergistically Enhance Antiadhesive Properties, ACS Appl. Mater. Interfaces. 11 (2019) 18090–18102. https://doi.org/10.1021/acsami.9b01493.